IEEE Access
Multidisciplinary | Rapid Review | Open Access Journal

Received January 25, 2021, accepted February 5, 2021, date of publication February 22, 2021, date of current version March 2, 2021.

Digital Object Identifier 10.1109/ACCESS.2021.3060784

NOMA Based Cooperative Relaying Strategy for Underwater Acoustic Sensor Networks Under Imperfect SIC and Imperfect CSI: A Comprehensive Analysis

VEERAPU GOUTHAM, (Member, IEEE), AND V. P. HARIGOVINDAN, (Senior Member, IEEE)
Department of Electronics and Communication Engineering, National Institute of Technology Puducherry, Karaikal 609609, India

Corresponding author: Veerapu Goutham (gouthamveerapu@gmail.com)

This work was supported by the Science Engineering Research Board, Department of Science and Technology, Government of India, through the Mathematical Research Impact Centric Support scheme under Grant MTR/2019/001228.

ABSTRACT In this paper, we propose non-orthogonal multiple access based cooperative relaying strategy (NOMA-CRS) for underwater acoustic sensor networks (UASNs). We analyse the performance of NOMA-CRS for both shallow and deep water scenarios, under imperfect channel state information (I-CSI) as well as imperfect successive interference cancellation (I-SIC). We derive mathematical expressions for ergodic rate, outage probability as well as the energy efficiency of NOMA-CRS in UASNs by considering the underwater specific characteristics, such as distance-dependent usable bandwidth, acoustic spreading, propagation loss, and fading effects. We compare the performance of NOMA-CRS with the widely used decode-and-forward based CRS in the UASNs. From the results, it is evident that NOMA-CRS can achieve significant improvement in ergodic sum rate and energy efficiency. But the outage performance is slightly degraded for the proposed scheme. Our results show that I-CSI and I-SIC have a significant impact on the performance of the NOMA-CRS. We also investigate the impact of relay position, wind speed as well as shipping activities on the performance of NOMA-CRS under the realistic underwater scenario. Results show that high-speed winds and high shipping activities severely degrade the performance of ergodic sum rate of the NOMA-CRS. Implementation of NOMA-CRS requires CSI at the transmitter. However, acquiring perfect CSI at the transmitter is a challenging task in time-varying multi-path underwater acoustic channels. As a solution, we also propose space-time block coded NOMA-CRS (STBC-NOMA-CRS) for UASNs, which can be implemented without CSI at the transmitter. Extensive simulation studies are conducted to corroborate the analytical findings.

INDEX TERMS Cooperative relaying strategy, ergodic rate, energy efficiency, outage probability, power-domain non-orthogonal multiple access, space-time block codes, underwater acoustic sensor networks.

I. INTRODUCTION

Recent advances in underwater wireless sensor networks (UWSNs) lead to a variety of oceanic applications, which include ocean exploration, underwater multimedia, military surveillance system, assisted navigation, pollution control, and much more. Nowadays, UWSNs also support the Internet of Things, which has been described as the Internet of underwater things (IoUT) [1]. IoUT consists of multiple underwater objects, which are interconnected through a wireless communication medium. In particular, IoUT allows applications to monitor the vast unexplored marine areas [1]–[3]. UWSNs may consist of both mobile and stationary nodes that exchange information, such as control, telemetry, speech, and video signals among themselves as well as to a central node located on or offshore. Such diverse and data-intensive underwater applications demand higher bandwidth as well as data rate [4]. Innovative physical (PHY) layer

The associate editor coordinating the review of this manuscript and approving it for publication was Giovanni Pau.

schemes are therefore needed to develop spectral efficient, highly reliable, and energy-efficient UWSN to meet these challenges. Underwater wireless communication is achieved either by radio frequency (RF) or by optical or by acoustic signals. Although RF signals have a significant bandwidth, they are extremely prone to absorption losses in the underwater medium. Optical signals face extreme challenges due to absorption losses, dispersion caused by suspended particles and ambient light interference. This leads to a low transmission range of a few meters with underwater optical communication. The wireless technology with acoustic signals is the preferred and most popular mode of communication in UWSNs due to its long-range data transmission. However, the use of acoustic signals in the PHY layer offers limited communication bandwidth, limited data rates and increased propagation delays compared to terrestrial wireless sensor networks (WSNs). Additionally, the underwater communication channel suffers from node mobility, multi-path fading and Doppler spread. All of these factors lead to variations in the temporal and spatial characteristics of the underwater acoustic sensor network (UASN) channel. This makes the channel bandwidth dependent on both transmission distance and signal frequency. Therefore, improving channel capacity within the limited communication bandwidth is one of the major concerns in UASNs.

To achieve higher data rates, massive multiple input multiple output (MIMO), and non-orthogonal multiple access (NOMA), are introduced in terrestrial communication systems [5]–[9]. However, practical implementation of massive MIMO over frequency-selective channels such as UASNs is a challenging task considering the higher complexity of the equalisers. Recently, NOMA is seen as a promising technique in UASNs to achieve higher data rates within the limited communication bandwidth. Authors in [10]–[14] proposed NOMA for UASNs to improve channel capacity. NOMA can be implemented by exploiting either power or code domains. Power-domain NOMA can transmit multiple user information within a single resource block by sharing the transmission power among the users. A resource block can be a time slot or a frequency band or a code. The key techniques involved in power-domain NOMA are superposition coding and successive interference cancellation (SIC). Further, authors in [15]–[17] combined the NOMA with a cooperative relaying strategy (NOMA-CRS) to improve the channel capacity and reliability of the terrestrial wireless systems. The authors of [17] analysed the impact of imperfect channel state information on the performance of NOMA with cooperative relaying for terrestrial wireless communications by considering perfect SIC. Although advanced SIC techniques can mitigate the impact of successive interference up to some extent, still near node will be affected by the residual successive interference from the higher power transmission symbols, which increases proportionally with the distance between near node and the source node. Besides, all recently published works on NOMA for UASNs have analysed the ergodic rate by assuming perfect CSI, which is too idealistic assumption in UASNs due to the underwater channel characteristics. This assumption does not provide clear insight into the performance of the practical UASN due to the existence of the channel estimation errors. It has been observed that the performance analysis of the NOMA scheme under I-CSI and I-SIC for UASNs has not yet reported in the literature.

On the other hand, CRS is a powerful approach in UASNs, that enhances the reliability and energy efficiency. In CRS, nearby relay nodes cooperate with the source node to improve the reliability by exploiting spatial diversity. Some of the existing research works have proposed the CRS for UASNs to enhance throughput, reliability and energy efficiency [4], [18]–[22]. Various types of CRS strategies are proposed for UASNs, namely amplify-and-forward and decode-and-forward [4], [23]. In amplify-and-forward CRS, the relay node amplifies the data received from the source node, and retransmits the information to the destination node [24]. Whereas in the decode-and-forward CRS, the relay node decodes the source node information, and retransmits decoded information to the destination node. The authors of [25] investigated the outage performance for cooperative orthogonal frequency division multiple access with both amplify-and-forward and decode-and-forward relaying strategies for underwater communication systems. Authors of [26] proposed energy-efficient cooperative opportunistic routing protocol for UASNs. Here, the source node uses the depth information of the underwater devices and residual energy of the relay nodes as constraints to determine the route to the destination node. CRS mechanisms are also designed for UASNs to address the medium access control layer and network layers issues, which mainly focus on enhancing energy efficiency of UASNs [27]–[29]. Most of these works have focused primarily on improving energy efficiency and reliability in bandwidth-limited UASNs with the cost of reduced ergodic rates. Differently from the existing works, in this research work, we aim to improve both ergodic sum rate and energy efficiency of UASNs within the limited bandwidth of the PHY layer by combining CRS with the NOMA. In addition, obtaining perfect CSI at the transmitter is a complex task in UASNs due to the long propagation delays. We therefore propose NOMA-CRS scheme, which can be implemented without CSI at the transmitter, by integrating the proposed scheme with the STBC codes. STBC codes are popular for the transmitter cooperation without CSI at the transmitter.

To the best of authors' knowledge, this is the first research work to analyse NOMA based CRS for UASNs under imperfect CSI as well as imperfect SIC and to propose space-time block coded NOMA-CRS (STBC-NOMA-CRS) for UASNs. The major contributions of this research work are as follows:

1) We propose non-orthogonal multiple access based cooperative relaying strategy (NOMA-CRS) for underwater acoustic sensor networks (UASNs).
2) We present a comprehensive study of NOMA-CRS for UASNs under imperfect channel state information

(I-CSI) and imperfect successive interference cancellation (I-SIC) in both shallow and deep water scenarios.
3) We derive mathematical expressions of ergodic rate, outage probability and energy efficiency for NOMA-CRS for UASNs by considering the underwater specific characteristics such as distance-dependent usable bandwidth and transmission power, acoustic spreading, propagation loss, and fading effects.
4) The performance of NOMA-CRS is compared with widely used decode-and-forward based CRS in the UASNs. The results show that the NOMA-CRS can achieve improved ergodic sum rate, and energy efficiency at the cost slightly reduced outage performance. The impact of I-CSI and I-SIC on the performance of NOMA-CRS is also thoroughly investigated.
5) We also examine the impacts of the relay position, and environmental effects such as, wind speed and shipping activities on the NOMA-CRS considering realistic underwater scenario. Results show that high-speed winds and high shipping activities severely degrade the performance of ergodic sum rate of the NOMA-CRS.
6) Acquiring perfect CSI at the transmitter is one of the major challenge in implementing NOMA in UASNs. As a solution to this, we propose space-time block coded NOMA-CRS (STBC-NOMA-CRS) for UASNs, which brings forth the opportunity to exploit the benefits of both spectral efficiency and transmit diversity.

The rest of the paper is organized as follows: Section II presents UASN model along with the proposed NOMA-CRS, and CRS schemes for UASNs. In this section, we also derive mathematical expressions for ergodic rate, outage probability and energy efficiency of NOMA-CRS scheme in UASNs. Section III presents STBC-NOMA-CRS for UASNs. Section IV provides a description of analytical and simulation results. The conclusion is presented in Section V.

II. SYSTEM MODEL

This section presents (1) the physical layer modeling of UASNs, (2) the proposed NOMA-CRS scheme for UASNs, and (3) the mathematical modeling and derivation of accurate expressions for the ergodic rate, the outage probability and the energy efficiency of NOMA-CRS for UASNs.

A. PHYSICAL LAYER MODEL

In this subsection, we present the physical layer model for the calculation of the SNR in UASNs [30], [31]. The signal-to-noise ratio (SNR) at the receiver of the UASNs is provided by the passive sonar equation. Using this equation, the SNR at the receiver can be calculated from the transmitted signal level (*i.e.,* source level (SL)), by considering transmission loss (TL), ambient noise level (NL), and directivity (DI) can be calculated. The passive sonar equation is given by,

$$\Gamma_{in\ dB} = SL - TL - (NL - DI), \tag{1}$$

where Γ is the expected SNR at the receiver in dB. SL measured at 1 m with respect to the reference intensity is given by,

$$SL = 10\log_{10} I_s - 10\log_{10} I_{ref} + 10\log_{10} \eta_{ea}, \tag{2}$$

where, I_s is the signal intensity transmitted from the source measured at 1 m distance, I_{ref} is the reference intensity, and η_{ea} is the electrical to acoustic power conversion efficiency. Here, we consider both shallow and deep water scenarios. The characteristics of shallow and deep water scenarios are given in Table. 1.

TABLE 1. Shallow and deep water characteristics.

Characteristics	Shallow water	Deep water
Depth in km	0 - 0.1	0.1 - 10
Transmission loss anomaly	surface reflection loss	Both surface and bottom reflection loss, sediment loss
Temperature	high ($24°C$)	low ($4°C$)
Salinity	35.5 ppt	34.5 ppt
Geometric spreading	cylindrical spreading	spherical spreading
Density $\left(\frac{kg}{m^3}\right)$	1.025	1.028

The transmitted signal intensity (I_s) is the power flow per unit area. The propagation of acoustic waves encounters the spherical spreading in deep water [30]. So, the signal intensity transmitted from the source in deep water is given by, $I_s = \frac{P_{tx}}{4\pi}$, where P_{tx} is the transmitted signal power from the source. Whereas, the propagation of acoustic waves encounters cylindrical spreading in the case of shallow water due to the signals being bounded by the floor and surface of the ocean. Hence, the signal intensity transmitted from the source in shallow water is given by, $I_s = \frac{P_{tx}}{2\pi H}$, where H is the water depth in meters. The term I_{ref} is the reference intensity, which is given by $\frac{q^2}{\rho c}$, where $q = 1\mu\ Pa\ rms$ is the root mean square acoustic pressure, ρ the density of sea water, and c is the sound velocity in sea. c is mainly affected by temperature, sea depth and salinity of sea water, and is given by [30], [32],

$$\begin{aligned} c = {} & 1448.96 + 4.591T - 0.05304T^2 + 0.0002374T^3 \\ & + 1.340(\chi - 35) + 0.0163H + 1.675 \times 10^{-7}H^2 \\ & - 0.01025T(\chi - 35) - 7.139 \times 10^{-13}TH^3, \end{aligned} \tag{3}$$

where T is the temperature, and χ is the salinity of sea water. TL consists of absorption and spreading losses. TL between transceiving nodes in an underwater acoustic channel is given by [33],

$$TL = k \times 10\log r + r \times 10^{-3} \times 10\log a(H, T, f) + A, \tag{4}$$

where k is the spreading factor, r is the distance between transceiving nodes in km, A is transmission loss anomaly and $a(H, T, f)$ is the absorption coefficient in dB/km for f in kHz. The Francois & Garrison model proposed in [34],and [35] is an accurate and most commonly used model for calculating the absorption coefficient in UASNs, which not only takes into account the effect of acoustic frequency but also introduces the effects of temperature (T), depth (H), pressure, acidity, and salinity (χ). In this research work, we use this

accurate absorption coefficient model. The absorption coefficient $a(H,T,f)$ in dB/km (valid for $100\ Hz < f < 1\ MHz$) is given by [34], [35],

$$a(H,T,f) = \frac{A_1 P_1 f_1 f^2}{f^2 + f_1^2} + \frac{A_2 P_2 f_2 f^2}{f^2 + f_2^2} + A_3 P_3 f^2, \quad (5)$$

where f is the operating signal frequency, f_1, and f_2 are the relaxation frequencies in kHz for boric acid and magnesium sulphate. $A_i\ i \in \{1,2,3\}$, and $P_i\ i \in \{1,2,3\}$ are the coefficients, which considers the effects of temperature, salinity and depth on acoustic signal absorption. The expressions for finding these coefficients are given by,

$$f_1 = 2.8\left(\frac{\chi}{35}\right)^{0.5} 10^{\left[4-\frac{1245}{273+T}\right]}$$

$$f_2 = \frac{8.17 \times 10^{\left[8-\frac{1990}{273+T}\right]}}{1 + 18 \times 10^{-4}(\chi - 35)}$$

$$A_1 = \frac{8.68}{c} \times 10^{(0.78\ pH-5)}$$

$$A_2 = 21.44(1 + 0.025\ T)\frac{\chi}{c}$$

$$A_3 = \begin{cases} 4.937\times10^{-4} - 2.59\times10^{-5}T + 9.11\times10^{-7}T^2 \\ +9.11\times10^{-7}T^2 - 1.50\times10^{-8}T^3\ for\ T \leq 20°C \\ 3.964\times10^{-4} - 1.146\times10^{-5}T + 1.45\times10^{-7}T^2 \\ -6.5\times10^{-10}T^3\ for\ T > 20°C \end{cases}$$

$$P_1 = 1$$

$$P_2 = 1 - 1.37\times10^{-4}H + 6.2\times10^{-9}H^2$$

$$P_3 = 1 - 3.83\times10^{-5}H + 4.9\times10^{-10}H^2. \quad (6)$$

Ambient noises in UASNs includes turbulence noise ($N_t(f)$), shipping noise ($N_s(f)$), waves noise ($N_w(f)$) and thermal noise ($N_{th}(f)$). The empirical formulas for the power spectral densities (expressed in dB re $1\mu\ Pa\ per\ Hz$) of these noise components are given by,

$$10\log_{10}N_t(f) = 17 - 30\log_{10}f, for f < 10\ Hz$$

$$10\log_{10}N_s(f) = \begin{cases} 40 + 20(s-0.5) + 26\log_{10}f \\ -60\log_{10}(f + 0.03), \\ for\ 10 < f < 100\ Hz \end{cases}$$

$$10\log_{10}N_w(f) = \begin{cases} 50 + 7.5w^{0.5} + 20\log_{10}f \\ -40\log_{10}(f + 0.4), \\ for\ 0.1\ kHz < f < 100\ kHz \end{cases}$$

$$10\log_{10}N_{th}(f) = -15 + 20\log_{10}f,\ for\ f > 100\ kHz, \quad (7)$$

where, w is the wind speed and s is the shipping activity. The ambient noise level generally decreases with increase in frequency. The sum of these four noise components gives the total power spectral density (p.s.d) of ambient noise ($N(f)$) present in the ocean. The approximate p.s.d of ambient noise present in the ocean is given by, $10\log_{10}(N(f)) = 50 - 18\log_{10}(f)$ [36]. In UASNs, noise and path losses are primarily dependent on the signal frequency (f) and the transmission distance (r). The achievable ergodic rate for frequency-dependent noise is therefore defined as [36], $C = E\left[\int_{B(r)} \log_2(1 + \Gamma(r,f))\, df\right]$, where $B(r)$ represents distance-dependent usable bandwidth, which is given by, $B(r) = Br^{-Q}$, and $E[\ ]$ is the expectation of the random variable. Here B is bandwidth coefficient and Q is positive bandwidth exponent.

B. NOMA-CRS SCHEME

We consider a simple three-terminal communication scenario as shown in Fig. 1, consisting of three half-duplex nodes. S is the source node, G is the near node to S with good channel conditions, and P is the node far from S with poor channel conditions. The distance between the S-to-P and S-to-G links are denoted as D_{SP}, and D_{SG}, respectively. The angle between the S-to-P and S-to-G links is denoted as θ. Using cosine rule, the distance between the G-to-P link is given by, $D_{GP} = \sqrt{D_{SP}^2 + D_{SG}^2 - 2\,D_{SP}\,D_{SG}\cos\theta}$. The channel coefficient of S-to-P link is expressed as $h_{SP} = |h_{SP}|e^{j\theta_{SP}}$, with an average power of β_{SP}, where $|h_{SP}|$ and θ_{SP} are the magnitude and phase of the S-to-P link, respectively. Similarly, the channel coefficients of S-to-G, and G-to-P links are expressed as $h_{SG} = |h_{SG}|e^{j\theta_{SG}}$, and $h_{GP} = |h_{GP}|e^{j\theta_{GP}}$, with average powers of β_{SG}, and β_{GP}, respectively. Channel coefficients h_{SP}, h_{SG}, and h_{GP} are assumed to be independent Rayleigh fading coefficients due to the multi-path signal propagation in UASNs. Accordingly, the channel powers $|h_{SP}|^2$, $|h_{SG}|^2$, and $|h_{GP}|^2$ are exponentially distributed random variables. It is assumed that the average power of the channel coefficient h_{SP} is less than the average power of the channel coefficient h_{SG} ($|h_{SP}|^2 < |h_{SG}|^2$), due to the high path loss of the S-to-P link compared to the S-to-G channel link. In UASNs, due to channel estimation errors, it is extremely difficult to obtain the perfect CSI [37], [38]. Hence, we consider the estimation of h_j is $\tilde{h}_j, j \in \{SP,\ SG,\ GP\}$, and the channel coefficient can be modelled as $\tilde{h}_j = h_j + \kappa\hat{h}_j$, where $\hat{h}_j$ represents channel error vector which can be modelled as zero mean complex normal distribution with variance of ν_j^2, and κ is the channel estimation error factor.

In NOMA-CRS, both the symbols X_1 and X_2 are intended to be transmitted to the node P as shown in Fig. 1. In NOMA-CRS scheme, the node S transmits two symbols X_1 and X_2 with distinct power levels $\alpha_1\ P_t$ and $\alpha_2\ P_t$ respectively, where P_t is the total transmission power, α_1 and α_2 are the power allocation coefficients ($\alpha_1 + \alpha_2 = 1$, $\alpha_1 > \alpha_2$). Here, the node G operates as a half-duplex decode-and-forward relay, which decodes the symbols using SIC technique. Then node G transmits the X_2 symbol to node P with the power P_t in the next transmission time slot as shown in Fig. 1. As a result, the node P can obtain the symbol X_2 through the S-to-G-to-P and S-to-P links. Subsequently, the node P decodes the symbols received from the S and G nodes jointly by involving selection combining diversity and successive interference cancellation techniques. Accordingly, the signal

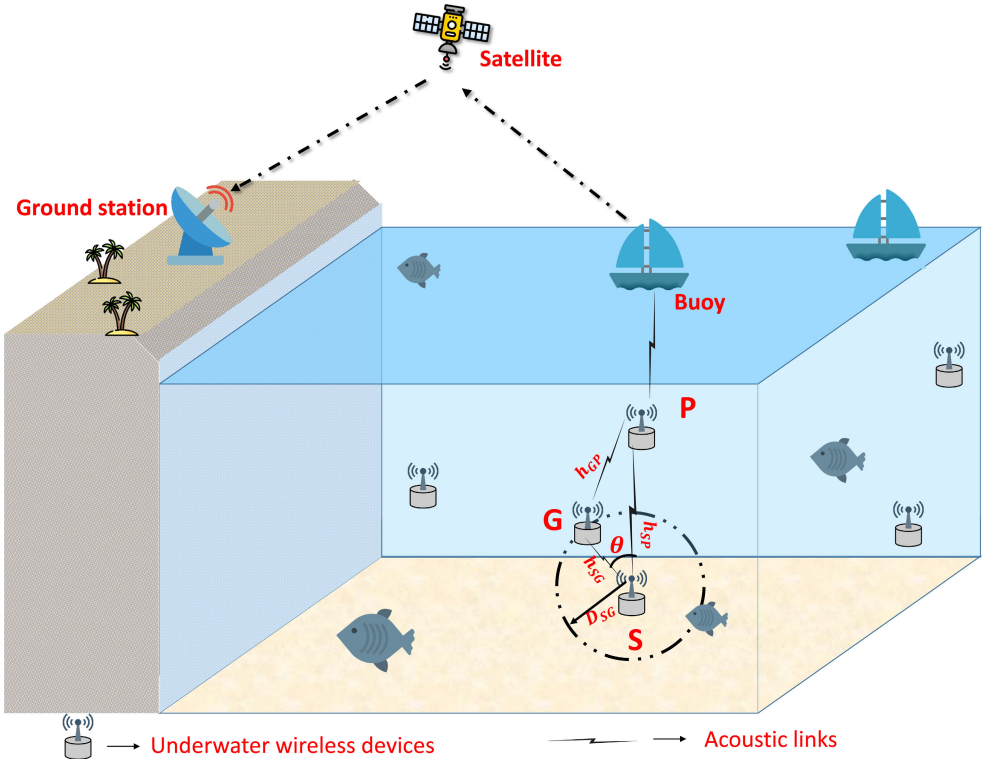

FIGURE 1. NOMA-CRS scheme for UASNs.

received at the node G in a given time slot i is expressed as,

$$Y_{SG}(i)=\left(\frac{h_{SG}+\kappa\hat{h}_{SG}}{\sqrt{TL_{SG}(r,f)}}\right)\left[\sqrt{a_1P_t}X_1(i)+\sqrt{a_2P_t}X_2(i)\right]+n_{SG}(i), \tag{8}$$

where $n_{SG}(i)$ denotes frequency dependent noise in the underwater channel with variance of $\sigma^2_{SG}(f)$. Firstly, the node G decodes symbol X_1. Then, it subtracts decoded symbol X_1 from $Y_{SG}(i)$ using SIC technique to obtain the symbol X_2. Therefore, the SINRs of both the symbols X_1 and X_2 at the node G are respectively expressed as,

$$\begin{aligned}\gamma^{X_1}_{SG} &= \frac{a_1|h_{SG}|^2\frac{P_t}{TL_{SG}(r,f)}}{a_2|h_{SG}|^2\frac{P_t}{TL_{SG}(r,f)}+\kappa^2\nu^2_{SG}\frac{P_t}{TL_{SG}(r,f)}+\sigma^2_{SG}(f)}\\ &= \frac{a_1|h_{SG}|^2\Gamma_{SG}}{a_2|h_{SG}|^2\Gamma_{SG}+\kappa^2\nu^2_{SG}\Gamma_{SG}+1},\end{aligned} \tag{9a}$$

$$\begin{aligned}\gamma^{X_2}_{SG} &= \frac{a_2|h_{SG}|^2\frac{P_t}{TL_{SG}(r,f)}}{\xi a_1|h_{SG}|^2\frac{P_t}{TL_{SG}(r,f)}+\kappa^2\nu^2_{SG}\frac{P_t}{TL_{SG}(r,f)}+\sigma^2_{SG}(f)}\\ &= \frac{a_2|h_{SG}|^2\Gamma_{SG}}{\xi a_1|h_{SG}|^2\Gamma_{SG}+\kappa^2\nu^2_{SG}\Gamma_{SG}+1},\end{aligned} \tag{9b}$$

where $\Gamma_{SG}=\frac{P_t}{TL_{SG}(r,f)\sigma^2_{SG}(f)}$ and the term $\xi a_1|h_{SG}|^2\Gamma_{SG}$ indicates the residual successive interference after SIC at the node G, and ξ denotes the SIC inefficiency. ξ varies in the range of $[0, 1]$, $\xi = 0$ represents perfect SIC and other values of ξ represent I-SIC *i.e.,* interference due to residual signals. Higher values of ξ indicates receiver with higher SIC inefficiency. The received signal at node P from S in a given time slot i is given by,

$$Y_{SP}(i)=\left(\frac{h_{SP}+\kappa\hat{h}_{SP}}{\sqrt{TL_{SP}(r,f)}}\right)\left[\sqrt{a_1P_t}X_1(i)+\sqrt{a_2P_t}X_2(i)\right]+n_{SP}(i), \tag{10}$$

where $n_{SP}(i)$ is the frequency dependent noise in the underwater channel with the variance of $\sigma^2_{SP}(f)$. Therefore, the signal-to-interference noise ratio (SINR) for X_1 symbol $\gamma^{X_1}_{SP}(r,f)$ at the node P is obtained by,

$$\begin{aligned}\gamma^{X_1}_{SP} &= \frac{a_1|h_{SP}|^2\frac{P_t}{TL_{SP}(r,f)}}{a_2|h_{SP}|^2\frac{P_t}{TL_{SP}(r,f)}+\kappa^2\nu^2_{SP}\frac{P_t}{TL_{SP}(r,f)}+\sigma^2_{SP}(f)}\\ &= \frac{a_1|h_{SP}|^2\Gamma_{SP}}{a_2|h_{SP}|^2\Gamma_{SP}+\kappa^2\nu^2_{SP}\Gamma_{SP}+1},\end{aligned} \tag{11}$$

where $\Gamma_{SP}=\frac{P_t}{TL_{SP}(r,f)\sigma^2_{SP}(f)}$. In the second transmission time slot, the node G transmits symbol X_2 to the node P. Hence, the received signal at node P from G in a given time slot i is given by,

$$Y_{GP}(i)=\left(\frac{h_{GP}+\kappa\hat{h}_{GP}}{\sqrt{TL_{GP}(r,f)}}\right)\left[\sqrt{P_t}X_2(i)\right]+n_P(i). \tag{12}$$

Here, we consider selection diversity at the node P. The node P combines the X_2 symbol from S and G using selection diversity technique. Therefore, the SINR for X_2 symbol

$\gamma_P^{X_2}(r,f)$ at the node P is obtained by,

$$\gamma_P^{X_2} = max\left\{\frac{a_2|h_{SP}|^2\Gamma_{SP}}{\xi a_1|h_{SP}|^2\Gamma_{SP}+\kappa^2\nu_{SP}^2\Gamma_{SP}+1}, \frac{|h_{GP}|^2\Gamma_{GP}}{\kappa^2\nu_{GP}^2\Gamma_{GP}+1}\right\}, \quad (13)$$

where $\Gamma_{GP} = \frac{P_t}{TL_{GP}(r,f)\sigma_{GP}^2(f)}$.

1) ERGODIC RATE

Let $E[Z]$, $F_Z(z)$, and $f_Z(z)$ denote the expectation, cumulative distribution function (CDF) and probability density function of a random variable Z, respectively. The ergodic rate of the X_1 symbol in NOMA-CRS scheme for UASNs is given by,

$$C_{X_1} = \frac{1}{2}\int_{fl}^{fu} E\left[\log_2\left(1+min\left\{\gamma_{SP}^{X_1}, \gamma_{SG}^{X_1}\right\}\right)\right]df. \quad (14)$$

where, fl and f_u are the lower and upper cutoff frequencies, and $\gamma_{SP}^{X_1}$ and $\gamma_{SG}^{X_1}$ are the respective SINR of symbol X_1 at S-to-P and S-to-G links. From (14), we assume V_1 is an arbitrary variable, considered as $V_1 = \log_2\left(1+min\left\{\gamma_{SP}^{X_1}, \gamma_{SG}^{X_1}\right\}\right)$. By substituting (11) and (9a), we obtain variable V_1 as,

$$V_1 = \log_2\left(1+min\left\{\frac{a_1|h_{SP}|^2\Gamma_{SP}}{a_2|h_{SP}|^2\Gamma_{SP}+\psi_{SP}}, \frac{a_1|h_{SG}|^2\Gamma_{SG}}{a_2|h_{SG}|^2\Gamma_{SG}+\psi_{SG}}\right\}\right), \quad (15)$$

where $\psi_{SP} = \kappa^2\nu_{SP}^2\Gamma_{SP}+1$ and $\psi_{SG} = \kappa^2\nu_{SG}^2\Gamma_{SG}+1$. Accordingly,

$$\begin{aligned} V_1 &= \log_2\left(1+min\left\{\frac{a_1}{a_2+\frac{\psi_{SP}}{|h_{SP}|^2\Gamma_{SP}}}, \frac{a_1}{a_2+\frac{\psi_{SG}}{|h_{SG}|^2\Gamma_{SG}}}\right\}\right), \\ &= \log_2\left(1+\frac{a_1}{a_2+\frac{1}{min\left\{\frac{|h_{SP}|^2\Gamma_{SP}}{\psi_{SP}}, \frac{|h_{SG}|^2\Gamma_{SG}}{\psi_{SG}}\right\}}}\right), \\ &= \log_2\left(1+min\left\{\frac{|h_{SP}|^2\Gamma_{SP}}{\psi_{SP}}, \frac{|h_{SG}|^2\Gamma_{SG}}{\psi_{SG}}\right\}\right) \\ &\quad -\log_2\left(1+min\left\{\frac{a_2|h_{SP}|^2\Gamma_{SP}}{\psi_{SP}}, \frac{a_2|h_{SG}|^2\Gamma_{SG}}{\psi_{SG}}\right\}\right). \end{aligned} \quad (16)$$

Let, U and V are random variables, which are denoted by, $U \triangleq \frac{|h_{SP}|^2\Gamma_{SP}}{\psi_{SP}}$, and $V \triangleq \frac{|h_{SG}|^2\Gamma_{SG}}{\psi_{SG}}$, respectively. Accordingly, the CDF of random variable U is given by, $F_U(u) = 1-e^{-\frac{u}{\beta_{SP}\Gamma_{SP}}\frac{\psi_{SP}}{}}$ and CDF of random variable V is given by, $F_V(v) = 1-e^{-\frac{v}{\beta_{SG}\Gamma_{SG}}\frac{\psi_{SG}}{}}$. We consider W is a random variable denoted by, $W \triangleq min\{U, V\}$. Based on the random variable transformations, the CDFs of W is obtained as,

$$F_W(w) = 1-e^{-w\left(\frac{1}{\lambda_{SP}}+\frac{1}{\lambda_{SG}}\right)}, \quad (17)$$

where $\lambda_{SP} = \frac{\beta_{SP}\Gamma_{SP}}{\psi_{SP}}$ and $\lambda_{SG} = \frac{\beta_{SG}\Gamma_{SG}}{\psi_{SG}}$. Let $X \triangleq a_2 W$. Based on the linear random variable transformation, the CDFs of X is obtained as, $F_X(x) = 1-e^{-x\left(\frac{1}{a_2}\frac{1}{\lambda_{SP}}+\frac{1}{a_2}\frac{1}{\lambda_{SG}}\right)}$. Using the random variables, W and X, (14) can be re-written as,

$$C_{X_1} = \frac{1}{2}\int_{fl}^{fu}\int_0^{\infty}\log_2(1+W)f_W(w)\,dw\,df - \frac{1}{2}\int_{fl}^{fu}\int_0^{\infty}\log_2(1+X)f_X(x)\,dx\,df. \quad (18)$$

By applying $\int_0^{\infty}\log_2(1+W)f_W(w)\,dw = \frac{1}{ln2}\int_0^{\infty}\frac{1-F_W(w)}{1+w}dw$, and $\int_0^{\infty}\frac{e^{-\mu x}}{x+\beta}dx = -e^{(\mu\beta)}Ei(-\mu\beta)$ [39], the ergodic rate for symbol X_1 is obtained as,

$$\begin{aligned} C_{X_1} &= \frac{1}{2\ln 2}\int_{fl}^{fu} -e^{\left(\frac{1}{\lambda_{SP}}+\frac{1}{\lambda_{SG}}\right)}Ei\left(-\frac{1}{\lambda_{SP}}-\frac{1}{\lambda_{SG}}\right)df \\ &\quad +\frac{1}{2\ln 2}\int_{fl}^{fu} e^{\frac{1}{a_2}\left(\frac{1}{\lambda_{SP}}+\frac{1}{\lambda_{SG}}\right)}Ei\left(-\frac{1}{a_2\lambda_{SP}}-\frac{1}{a_2\lambda_{SG}}\right)df. \end{aligned} \quad (19)$$

Similarly, the ergodic rate for X_2 symbol is given by,

$$C_{X_2} = \frac{1}{2}\int_{fl}^{fu} E\left[\log_2\left(1+min\left\{\gamma_P^{X_2}, \gamma_{SG}^{X_2}\right\}\right)\right]df. \quad (20)$$

From (20), V_2 is assumed as an arbitrary variable given by $V_2 = \log_2\left(1+min\left\{\gamma_P^{X_2}, \gamma_{SG}^{X_2}\right\}\right)$. By substituting (13) and (9b), we obtain variable V_2 as,

$$V_2 = \log_2\left(1+min\left\{max\left\{\frac{a_2|h_{SP}|^2\Gamma_{SP}}{\xi a_1|h_{SP}|^2\Gamma_{SP}+\psi_{SP}}, \frac{|h_{GP}|^2\Gamma_{GP}}{\psi_{GP}}\right\}, \frac{a_2|h_{SG}|^2\Gamma_{SG}}{\xi a_2|h_{SG}|^2\Gamma_{SG}+\psi_{SG}}\right\}\right), \quad (21)$$

where $\psi_{GP} = \kappa^2\nu_{GP}^2\Gamma_{GP}+1$. We assume Y and Z are random variables, which are denoted as, $Y \triangleq max\left\{\frac{a_2|h_{SP}|^2\Gamma_{SP}}{\xi a_1|h_{SP}|^2\Gamma_{SP}+\psi_{SP}}, \frac{|h_{GP}|^2\Gamma_{GP}}{\psi_{GP}}\right\}$, and $Z \triangleq \frac{a_2|h_{SG}|^2\Gamma_{SG}}{\xi a_2|h_{SG}|^2\Gamma_{SG}+\psi_{SG}}$. The corresponding CDFs of Y and Z are given by,

$$F_Y(y) = \begin{cases}\left(1-e^{-\frac{y\psi_{SP}}{\beta_{SP}\Gamma_{SP}(a_2-y\xi a_1)}}\right)\left(1-e^{-\frac{y\psi_{GP}}{\beta_{GP}\Gamma_{GP}}}\right); & y < \frac{a_2}{\xi a_1} \\ 1; & y \geq \frac{a_2}{\xi a_1}, \end{cases} \quad (22)$$

$$F_Z(z) = \begin{cases}\left(1-e^{-\frac{z\psi_{SG}}{\beta_{SG}\Gamma_{SG}(a_2-z\xi a_1)}}\right); & z < \frac{a_2}{\xi a_1} \\ 1; & z \geq \frac{a_2}{\xi a_1}. \end{cases} \quad (23)$$

Let, $A \triangleq min\{Y, Z\}$, and the CDF is obtained as,

$$F_A(a) = \begin{cases}1-(1-F_Y(a))(1-F_Z(a)); & a < \frac{a_2}{\xi a_1}, \\ 1; & a \geq \frac{a_2}{\xi a_1}. \end{cases} \quad (24)$$

Using the random variable A, (20) can be re-written as,

$$\begin{aligned} C_{X_2} &= \frac{1}{2}\int_{f_l}^{f_u}\int_{0}^{\infty} \log_2(1+A) f_A(a)\, da\, df \\ &= \frac{1}{2\ln 2}\int_{f_l}^{f_u}\int_{0}^{\infty} \frac{1-F_A(a)}{1+a}\, da\, df \\ &= \frac{1}{2\ln 2}\int_{f_l}^{f_u}\int_{0}^{\frac{a_2}{\xi a_1}} \frac{(1-F_Y(a))\,(1-F_Z(a))}{1+a} da\, df. \end{aligned} \tag{25}$$

The ergodic sum rate in NOMA-CRS for UASNs is given by, $C_{X_1} + C_{X_2}$.

2) OUTAGE PROBABILITY

In this subsection, the performance of NOMA-CRS for UASNs is analysed in terms of outage probability. It is defined as the instance where the received power level is less than the threshold power level, i.e. the receiver node is out of the source node range. Let R_1 and R_2 are the desired rates of X_1 and X_2 respectively. The mathematical expression for the outage probability of X_1 is given by,

$$P_{out}^{X_1} = Pr\left\{\frac{1}{2}\int_{f_l}^{f_u} \log_2\left(1+min\left\{\gamma_{SP}^{X_1}, \gamma_{SG}^{X_1}\right\}\right) df < R_1\right\}. \tag{26}$$

However, obtaining the mathematical expression for outage probability for frequency selective channels is tedious task. So, we formulate the problem as follows, we divide the total bandwidth into L narrow sub-bands. Let j^{th} sub-band be centered around frequency f_j with width δf_j, where $j = 1, 2, \cdots, L$. We assume each sub band is small enough such that the channel appears frequency-flat fading channel. As a result, the mathematical expression for average outage probability of X_1 symbol over L flat fading channels is given by,

$$\begin{aligned} P_{out}^{X_1} &= \frac{1}{L}\sum_{j=1}^{L} Pr\left\{\delta f_j \log_2\left(1+min\left\{\gamma_{SP}^{X_1}, \gamma_{SG}^{X_1}\right\}\right) < R_1\right\} \\ &= \frac{1}{L}\sum_{j=1}^{L}\left[1 - Pr\left\{min\left\{\gamma_{SP}^{X_1}, \gamma_{SG}^{X_1}\right\} \geq \Phi_1\right\}\right] \\ &= \frac{1}{L}\sum_{j=1}^{L}\left[1 - Pr\left\{|h_{SP}|^2 < \frac{\psi_{SP}\,\Phi_1}{a_1\Gamma_{SP} - a_2\Gamma_{SP}\,\Phi_1}\right\}\right. \\ &\quad \left. Pr\left\{|h_{SG}|^2 < \frac{\psi_{SG}\,\Phi_1}{a_1\Gamma_{SG} - a_2\Gamma_{SG}\,\Phi_1}\right\}\right] \\ &= \frac{1}{L}\sum_{j=1}^{L}\left[1 - \left(1 - e^{-\left(\frac{\psi_{SP}\,\Phi_1}{\beta_{SP}\Gamma_{SP}(a_1 - a_2\,\Phi_1)}\right)}\right)\right. \\ &\quad \left.\left(1 - e^{-\left(\frac{\psi_{SG}\,\Phi_1}{\beta_{SG}\Gamma_{SG}(a_1 - a_2\,\Phi_1)}\right)}\right)\right], \end{aligned} \tag{27}$$

where $\Phi_1 = 2^{\frac{2R_1}{\delta f_j}} - 1$. Similarly, the mathematical expression for average outage probability of X_2 symbol over L flat fading channels is given by, (28) as shown at the bottom of the page, where $\Phi_2 = 2^{\frac{2R_2}{\delta f_j}} - 1$.

C. CRS SCHEME

Decode-and-forward based CRS scheme is widely used scheme in UASNs for improving the energy efficiency and reliability [4], [21]. Here, the relay node is half-duplex, which completely decodes the source node information and retransmits it to the destination node in the next time slot. The destination node combines the two symbols received from the relay and source nodes using selection combining diversity technique. Accordingly, the average achieved ergodic rate by the decode-and-forward CRS is given by, (29) as shown at the bottom of the page,

$$\begin{aligned} P_{out}^{X_2} &= Pr\left\{\frac{1}{2}\int_{f_l}^{f_u} \log_2\left(1+min\left\{\gamma_P^{X_2}, \gamma_{SG}^{X_2}\right\}\right) df < R_2\right\} \\ &= \frac{1}{L}\sum_{j=1}^{L}\left[1 - Pr\left\{max\left\{\frac{a_2|h_{SP}|^2\Gamma_{SP}}{\xi a_1|h_{SP}|^2\Gamma_{SP} + \psi_{SP}}, \frac{|h_{GP}|^2\Gamma_{GP}}{\psi_{GP}}\right\} \geq \Phi_2\right\} Pr\left\{\frac{a_2|h_{SG}|^2\Gamma_{SG}}{\xi a_1|h_{SG}|^2\Gamma_{SG} + \psi_{SG}} \geq \Phi_2\right\}\right] \\ &= \frac{1}{L}\sum_{j=1}^{L}\left[1 - \left(1 - \left(1 - e^{-\left(\frac{\Phi_2\psi_{SP}}{\beta_{SP}\Gamma_{SP}(a_2 - \xi a_1\,\Phi_2)}\right)}\right)\left(1 - e^{-\left(\frac{\psi_{GP}\Phi_2}{\beta_{GP}\Gamma_{GP}}\right)}\right)\right)\left(1 - e^{-\left(\frac{\Phi_2\psi_{SG}}{\beta_{SG}\Gamma_{SG}(a_2 - \xi a_1\,\Phi_2)}\right)}\right)\right], \end{aligned} \tag{28}$$

$$\begin{aligned} C_{CRS} &= \frac{1}{2}\int_{f_l}^{f_u} E\left[\log_2\left(1+min\left\{\frac{\Gamma_{SG}\,|h_{SG}|^2}{\kappa^2 v_{SG}^2\Gamma_{SG}+1},\ max\left\{\frac{\Gamma_{SP}\,|h_{SP}|^2}{\kappa^2 v_{SP}^2\Gamma_{SP}+1}, \frac{\Gamma_{GP}\,|h_{GP}|^2}{\kappa^2 v_{GP}^2\Gamma_{GP}+1}\right\}\right\}\right)\right] df. \\ &= \frac{1}{2\ln 2}\int_{f_l}^{f_u}\int_{0}^{\infty} \frac{\left(1 - \left(1 - e^{-\frac{x\psi_{SG}}{\Gamma_{SG}}}\right)\left(1 - e^{-\frac{x\psi_{SP}}{\Gamma_{SP}}}\right)\right)\left(1 - e^{-\frac{x\psi_{GP}}{\Gamma_{GP}}}\right)}{1+b} db\, df \end{aligned} \tag{29}$$

Similarly, the outage probability for the decode-and-forward CRS scheme is given by,

$$P_{out}^{CRS} = \frac{1}{L}\sum_{j=1}^{L}\left[1-\left(1-\left(1-e^{-\frac{x\psi_{SG}}{\Gamma_{SG}}}\right)\left(1-e^{-\frac{x\psi_{SP}}{\Gamma_{SP}}}\right)\right)\left(1-e^{-\frac{x\psi_{GP}}{\Gamma_{GP}}}\right)\right]. \quad (30)$$

D. ENERGY EFFICIENCY

In this subsection, the performance of NOMA-CRS scheme is analysed from the perspective of energy efficiency. The expression for energy efficiency is given by [40],

$$\eta = \frac{(1-P_{out}^{X_1})\,C_{X_1} + (1-P_{out}^{X_2})\,C_{X_2}}{\text{Total power consumption}}. \quad (31)$$

The total power consumed in the NOMA-CRS scheme is given by, $E = 2P_t + 2P_{rx}$, where P_{rx} are the power consumed for receiving the symbols. Whereas, the total power consumed in the CRS scheme is given by, $E = 2P_t + 2P_{rx}$.

III. STBC-NOMA-CRS SCHEME

Even though NOMA based UASNs are proposed in the literature to improve the performance of UASNs, researchers identified that the major challenge in the implementation of NOMA in UASNs is that, the transmitter needs the prior CSI status encountered by each receiver. However, acquiring perfect CSI at the transmitter is a challenging job in time-varying multi-path underwater acoustic channels. In some cases, the transmitter obtains CSI using a feedback signal from the receiver in UASNs, where the receiver estimates CSI using receiving a pilot signal from the transmitter. Many recent research works proposed NOMA for UASNs, by assuming perfect or statistical CSI at the transmitter. But this assumption is too idealistic in UASNs. Differently, we propose space-time block coded NOMA-CRS (STBC-NOMA-CRS) for UASNs. To the best of authors' knowledge, this is the first work to propose, NOMA with STBC codes for UASNs. Since NOMA facilitates multiple transmissions simultaneously in the resource block, its inclusion with the space-time block codes (STBC) brings forth the opportunity to exploit the benefits of both spectral efficiency and transmit diversity.

To implement STBC with NOMA-CRS, we consider that, source node S is equipped with two transmitting antennas (*i.e.,* TX_1 & TX_2), node P equipped with one receiving antenna (*i.e.,* RX_1), and node G equipped with two transmitting antennas and one receiving antenna (*i.e.,* TX_3 , TX_4 & RX_2) as shown in Fig. 2. Let h_{11}, h_{12}, h_{21}, h_{22}, h_{13}, and h_{14} denote the channel coefficients of $TX_1 - RX_1$, $TX_2 - RX_1$, $TX_1 - RX_2$, $TX_2 - RX_2$, $TX_3 - RX_1$, and $TX_4 - RX_1$ links respectively. We model that all channels are independent and identically distributed Rayleigh fading channels because of the multi-path propagation of the acoustic signals in underwater communication. As a result, $|h_{11}|^2$, $|h_{12}|^2$, $|h_{21}|^2$, $|h_{22}|^2$, $|h_{13}|^2$, and $|h_{14}|^2$ are exponentially distributed random variables with average power of β_{11}, β_{12}, β_{21}, β_{22}, β_{13} and β_{14} respectively.

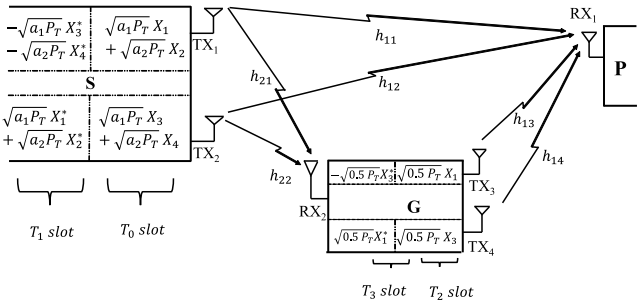

FIGURE 2. An illustration of STBC-NOMA-CRS scheme for UASNs.

The protocol description of the STBC-NOMA-CRS scheme for UASNs is as follows: the node S divides its transmission symbol stream $X(t)$ into four blocks, $X_1(t)$, $X_2(t)$, $X_3(t)$ and $X_4(t)$. Here, $X_1(t)$ & $X_3(t)$ are intended to be transmitted to the node P and $X_2(t)$ & $X_4(t)$ are intended to be transmitted to the node G simultaneously. As a result, the S combines $X_1(t)$ & $X_2(t)$ to form a composite signal $C_1(t)$, which is given by $C_1(t) = \sqrt{a_1P_t}\,X_1 + \sqrt{a_2P_t}\,X_2$, where a_1 & a_2 are power allocation coefficients. It is assumed that the total transmit power, from the two antennas in the STBC-NOMA-CRS scheme, is same as the transmit power from the NOMA-CRS scheme. As a result, we assume $a_1 + a_2 = 0.5$. Similarly, the S combines $X_3(t)$ & $X_4(t)$ to form an other composite signal $C_2(t)$, which is given by $C_2(t) = \sqrt{a_1P_t}\,X_3 + \sqrt{a_2P_t}\,X_4$. At the first transmission time slot (T_0), the signal transmitted from the TX_1 is $C_1(t)$ and from TX_2 is $C_2(t)$. During the next transmission time slot (T_1), signal $-C_2^*(t)$ is transmitted from the TX_1 and $C_1^*(t)$ is transmitted from the TX_2, where $*$ represents conjugate of the complex signal. Assuming that fading is constant across two consecutive symbols. The received signals at the G (*i.e., RX*$_2$) and P (*i.e., RX*$_1$) nodes in a given time slot i can then be expressed as,

$$\begin{aligned} Y_i(t) &= \left(\frac{h_{i1}+\kappa\hat{h}_{i1}}{\sqrt{TL_{i1}(r,f)}}\right)\left[\sqrt{a_1P_t}X_1(t)+\sqrt{a_2P_t}X_2(t)\right] \\ &\quad + \left(\frac{h_{i2}+\kappa\hat{h}_{i2}}{\sqrt{TL_{i2}(r,f)}}\right)\left[\sqrt{a_1P_t}X_3(t)+\sqrt{a_2P_t}X_4(t)\right]+n_i(t), \end{aligned} \quad (32)$$

where $i \in 1, 2$. Here $TL_{ij}(r,f)$ denotes transmission loss between j^{th} transmitter and i^{th} receiver and $n_i(t)$ denotes frequency dependent noise in the underwater channel. The received signals at the G and P nodes in the next transmission time slot (i+1) can then be expressed as,

$$\begin{aligned} Y_{i+1}(t) &= \left(\frac{h_{i1}+\kappa\hat{h}_{i1}}{\sqrt{TL_{i1}(r,f)}}\right)\left[-\sqrt{a_1P_t}X_3^*(t)-\sqrt{a_2P_t}X_4^*(t)\right] \\ &\quad + \left(\frac{h_{i2}+\kappa\hat{h}_{i2}}{\sqrt{TL_{i2}(r,f)}}\right)\left[\sqrt{a_1P_t}X_1^*(t)+\sqrt{a_2P_t}X_2^*(t)\right]+n_i(t). \end{aligned} \quad (33)$$

For decoding the symbols, STBC decoding algorithm can be applied to separate the composite signals (*i.e.,* $C_1(t)$ & $C_2(t)$) at both the nodes G and P. The STBC decoding algorithm performs maximum-likelihood detection with linear complexity. Subsequently, the node P does not perform successive interference cancellation (SIC) because of poor channel quality between $TX_1 - RX_1$ compared to $TX_1 - RX_2$. For decoding the symbols $X_1(t)$ & $X_3(t)$, the node P treats the symbols $X_2(t)$ & $X_4(t)$ as noise signals. As a result, the received signal-to-interference noise ratio (SINR) at RX_1 for symbol X_1 can be given by,

$$\gamma_{SP}^{X_1} = \frac{a_1 \left(\sum_{i=1}^{2} |h_{1i}|^2 \, \Gamma_{1i} \right)}{a_2 \left(\sum_{i=1}^{2} |h_{1i}|^2 \, \Gamma_{1i} \right) + \psi_1}, \tag{34}$$

where, $\psi_1 = \kappa^2 \nu_{11}^2 \Gamma_{11} + \kappa^2 \nu_{12}^2 \Gamma_{12} + 1$. Later, the near node decodes symbol $X_2(t)$ & $X_4(t)$ by performing the SIC. Firstly, the node G decodes $X_1(t)$ & $X_3(t)$ symbols by considering $X_2(t)$ & $X_4(t)$ as noise signals. Later, it subtracts decoded symbols $X_1(t)$ & $X_3(t)$ symbols from composite signals using SIC technique to obtain $X_2(t)$ & $X_4(t)$ symbols. The received SINRs at RX_2 for symbols X_1 & X_2 are given by,

$$\gamma_{SG}^{X_1} = \frac{a_1 \left(\sum_{i=1}^{2} |h_{2i}|^2 \, \Gamma_{2i} \right)}{a_2 \left(\sum_{i=1}^{2} |h_{2i}|^2 \, \Gamma_{2i} \right) + \psi_2}, \tag{35}$$

$$\gamma_{SG}^{X_2} = \frac{a_2 \left(\sum_{i=1}^{2} |h_{2i}|^2 \, \Gamma_{2i} \right)}{a_1 \xi \left(\sum_{i=1}^{2} |h_{2i}|^2 \, \Gamma_{2i} \right) + \psi_2}, \tag{36}$$

where, $\psi_2 = \kappa^2 \nu_{21}^2 \Gamma_{21} + \kappa^2 \nu_{22}^2 \Gamma_{22} + 1$ and ξ denotes the SIC inefficiency. ξ varies in the range of $[0, 1]$, $\xi = 0$ represents perfect SIC and other values represent imperfect SIC with inefficiency of ξ. Due to the symmetry in transmission scheme, $\gamma_{SG}^{X_1} = \gamma_{SG}^{X_3}$ & $\gamma_{SG}^{X_2} = \gamma_{SG}^{X_4}$.

At the next transmission time slot (T_2), the signal transmitted from the TX_3 is $\sqrt{0.5 P_t} X_2(t)$ and from TX_4 is $\sqrt{0.5 P_t} X_4(t)$. During the next transmission time slot (T_3), signal $-\sqrt{0.5 P_t} X_4^*(t)$ is transmitted from the TX_3, and $\sqrt{0.5 P_t} X_2^*(t)$ is transmitted from the TX_4. The received signals at the node P in a given time slot i+2 can then be expressed as,

$$Y_{i+2}(t) = \left(\frac{h_{i3} + \kappa \hat{h}_{i3}}{\sqrt{TL_{i3}(r,f)}} \right) \left[\sqrt{0.5 * P_t} X_2(t) \right] + \left(\frac{h_{i4} + \kappa \hat{h}_{i4}}{\sqrt{TL_{i4}(r,f)}} \right) \left[\sqrt{0.5 * P_t} X_4(t) \right] + n_i(t), \tag{37}$$

where $i \in 1$. The received signals at the node P in the next transmission time slot (i+3) can then be expressed as,

$$Y_{i+3}(t) = \left(\frac{h_{i3} + \kappa \hat{h}_{i3}}{\sqrt{TL_{i3}(r,f)}} \right) \left[-\sqrt{0.5 * P_t} X_4^*(t) \right] + \left(\frac{h_{i4} + \kappa \hat{h}_{i4}}{\sqrt{TL_{i4}(r,f)}} \right) \left[\sqrt{0.5 * P_t} X_2^*(t) \right] + n_i(t). \tag{38}$$

The received SINRs at RX_1 are given by,

$$\gamma_P^{X_2} = max \left\{ \frac{a_2 \left(\sum_{i=1}^{2} |h_{1i}|^2 \, \Gamma_{1i} \right)}{a_1 \xi \left(\sum_{i=1}^{2} |h_{1i}|^2 \, \Gamma_{1i} \right) + \psi_1} + \left(\frac{|h_{13}|^2 \, \Gamma_{13} + |h_{14}|^2 \, \Gamma_{14}}{2 \, \psi_1} \right) \right\}, \tag{39}$$

where, $\psi_1 = \kappa^2 \nu_{13}^2 \Gamma_{13} + \kappa^2 \nu_{14}^2 \Gamma_{14} + 1$. Due to the symmetry in transmission scheme, the SINR and ergodic rates achieved by symbol X_3 is exactly equal to X_1 and X_4 is equal to that of X_2.

A. ERGODIC RATE ANALYSIS

The ergodic rate of the X_1 symbol in STBC-NOMA-CRS scheme in UASNs is given by,

$$C_{X_1} = \frac{1}{4} \int_{f_l}^{f_u} E \left[\log_2 \left(1 + min \left\{ \gamma_{SP}^{X_1}, \gamma_{SG}^{X_1} \right\} \right) \right] df, \tag{40}$$

where $\gamma_{SP}^{X_1}$, and $\gamma_{SG}^{X_1}$ are the SINRs in UASNs at S and G nodes calculated by using (34) and (35), respectively. From (40), we assume $\tilde{V}_1$ is an arbitrary variable, considered as $\tilde{V}_1 = \log_2 \left(1 + min \left\{ \gamma_{SP}^{X_1}, \gamma_{SG}^{X_1} \right\} \right)$. By substituting (34) and (35), we obtain variable $\tilde{V}_1$ as,

$$\begin{aligned} \tilde{V}_1 &= \log_2 \left(1 + min \left\{ \frac{a_1 \left(\sum_{i=1}^{2} |h_{1i}|^2 \, \Gamma_{1i} \right)}{a_2 \left(\sum_{i=1}^{2} |h_{1i}|^2 \, \Gamma_{1i} \right) + \psi_1}, \right. \right. \\ &\qquad \left. \left. \frac{a_1 \left(\sum_{i=1}^{2} |h_{2i}|^2 \, \Gamma_{2i} \right)}{a_2 \left(\sum_{i=1}^{2} |h_{2i}|^2 \, \Gamma_{2i} \right) + \psi_2} \right\} \right) \\ &= \log_2 \left(1 + min \left\{ \sum_{i=1}^{2} \frac{|h_{1i}|^2 \, \Gamma_{1i}}{\psi_1}, \sum_{i=1}^{2} \frac{|h_{2i}|^2 \, \Gamma_{2i}}{\psi_2} \right\} \right) \\ &\quad - \log_2 \left(1 + a_2 min \left\{ \sum_{i=1}^{2} \frac{|h_{1i}|^2 \, \Gamma_{1i}}{\psi_1}, \sum_{i=1}^{2} \frac{|h_{2i}|^2 \, \Gamma_{2i}}{\psi_2} \right\} \right). \end{aligned} \tag{41}$$

Let, $\tilde{U}$ and $\tilde{V}$ are random variables denoted by, $\tilde{U} \triangleq \sum_{i=1}^{2} \frac{|h_{1i}|^2 \, \Gamma_{1i}}{\psi_1}$, and $\tilde{V} \triangleq \sum_{i=1}^{2} \frac{|h_{2i}|^2 \, \Gamma_{2i}}{\psi_2}$, respectively. Accordingly

the CDFs of random variable $\tilde{U}$ and $\tilde{V}$ are obtained as $F_{\tilde{U}}(u) = 1 - \frac{\lambda_{11}}{\lambda_{11}-\lambda_{12}} e^{-\frac{u}{\lambda_{11}}} + \frac{\lambda_{12}}{\lambda_{11}-\lambda_{12}} e^{-\frac{u}{\lambda_{12}}}$, $F_{\tilde{V}}(v) = 1 - \frac{\lambda_{21}}{\lambda_{21}-\lambda_{22}} e^{-\frac{u}{\lambda_{21}}} + \frac{\lambda_{22}}{\lambda_{21}-\lambda_{22}} e^{-\frac{u}{\lambda_{22}}}$, where $\lambda_{ij} = \frac{\beta_{ij}\Gamma_{ij}}{\psi_{ij}}$. We consider $\tilde{W}$ is a random variable denoted by, $\tilde{W} \triangleq min\left\{\tilde{U}, \tilde{V}\right\}$. Based on the random variable transformations, the CDFs of $\tilde{W}$ is obtained as,

$$F_{\tilde{W}}(w) = 1 - \left(\frac{\lambda_{11}}{\lambda_{11}-\lambda_{12}} e^{-\frac{u}{\lambda_{11}}} - \frac{\lambda_{12}}{\lambda_{11}-\lambda_{12}} e^{-\frac{u}{\lambda_{12}}}\right) \left(\frac{\lambda_{21}}{\lambda_{21}-\lambda_{22}} e^{-\frac{u}{\lambda_{21}}} - \frac{\lambda_{22}}{\lambda_{21}-\lambda_{22}} e^{-\frac{u}{\lambda_{22}}}\right). \quad (42)$$

Let $\tilde{X} \triangleq a_2\, \tilde{W}$. Based on the linear random variable transformation, the CDFs of $\tilde{X}$ is obtained as, $F_{\tilde{X}}(x) = F_{\tilde{W}}(\frac{x}{a_2})$. Using the random variables $\tilde{W}$, and $\tilde{X}$, (14) can be re-written respectively as,

$$C_{X_1} = \frac{1}{4}\int_{f_l}^{f_u}\int_0^{\infty} \log_2\left(1+\tilde{W}\right) f_{\tilde{W}}(w)\, dw\, df - \frac{1}{4}\int_{f_l}^{f_u}\int_0^{\infty} \log_2\left(1+\tilde{X}\right) f_{\tilde{X}}(x)\, dx\, df. \quad (43)$$

The mathematical expression for ergodic rate for symbol X_1 is obtained as,

$$\begin{aligned} C_{X_1} = C_1 \Bigg[&\int_{f_l}^{f_u} -\lambda_{11}\lambda_{21} e^{\left(\frac{1}{\lambda_{11}}\frac{1}{\lambda_{21}}\right)} Ei\left(-\frac{1}{\lambda_{11}} + \frac{1}{\lambda_{21}}\right) df \\ &+ \int_{f_l}^{f_u} -\lambda_{11}\lambda_{22} e^{\left(\frac{1}{\lambda_{11}}+\frac{1}{\lambda_{22}}\right)} Ei\left(-\frac{1}{\lambda_{11}} + \frac{1}{\lambda_{22}}\right) df \\ &+ \int_{f_l}^{f_u} -\lambda_{12}\lambda_{21} e^{\left(\frac{1}{\lambda_{12}}+\frac{1}{\lambda_{21}}\right)} Ei\left(-\frac{1}{\lambda_{12}} + \frac{1}{\lambda_{21}}\right) df \\ &- \int_{f_l}^{f_u} -\lambda_{12}\lambda_{22} e^{\left(\frac{1}{\lambda_{12}}+\frac{1}{\lambda_{22}}\right)} Ei\left(-\frac{1}{\lambda_{12}} + \frac{1}{\lambda_{22}}\right) df \Bigg], \end{aligned} \quad (44)$$

where $C_1 = \frac{1}{4\ln 2(\lambda_{11}-\lambda_{12})(\lambda_{21}-\lambda_{22})}$.

Similarly, the ergodic rate for X_2 symbol is given by,

$$C_{X_2} = \frac{1}{4}\int_{f_l}^{f_u} E\left[\log_2\left(1 + min\left\{\gamma_P^{X_2}, \gamma_{SG}^{X_2}\right\}\right)\right] df. \quad (45)$$

From (45), we assume $\tilde{V}_2$ is an arbitrary variable, considered as $\tilde{V}_2 = \log_2\left(1 + min\left\{\gamma_P^{X_2}, \gamma_{SG}^{X_2}\right\}\right)$. By substituting (39) and (36), we obtain variable $\tilde{V}_2$ as, (46) as shown at the bottom of the page.

We assume $\tilde{Y}$ and $\tilde{Z}$ are random variables, which are denoted as, $\tilde{Y} \triangleq \left(\frac{|h_{13}|^2\,\Gamma_{13}+|h_{14}|^2\,\Gamma_{14}}{2\,\tilde{\psi}_1}\right)$, and $\tilde{Z}_j \triangleq \frac{a_2\left(\sum_{i=1}^{2}|h_{ji}|^2\,\Gamma_{ji}\right)}{a_1\xi\left(\sum_{i=1}^{2}|h_{ji}|^2\,\Gamma_{ji}\right)+\psi_j}$, $j \in \{1,2\}$. The corresponding CDFs of $\tilde{Y}$ and $\tilde{Z}_j$ are given by,

$$F_{\tilde{Y}}(y) = 1 - \frac{\tilde{\lambda}_{13}}{\tilde{\lambda}_{13}-\tilde{\lambda}_{14}} e^{\frac{-y}{\tilde{\lambda}_{13}}} + \frac{\tilde{\lambda}_{14}}{\tilde{\lambda}_{13}-\tilde{\lambda}_{14}} e^{\frac{-y}{\tilde{\lambda}_{14}}}. \quad (47)$$

$$F_{\tilde{Z}_j}(z) = \begin{cases} 1 + \frac{\lambda_{j2}}{\lambda_{j1}-\lambda_{j2}} e^{-\frac{z}{a_2\lambda_{j2}-\xi a_1\lambda_{j2}z}} \\ -\frac{\lambda_{j1}}{\lambda_{j1}-\lambda_{j2}} e^{-\frac{z}{a_2\lambda_{j1}-\xi a_1\lambda_{j1}z}}; & z < \frac{a_2}{\xi a_1} \\ 1; & z \geq \frac{a_2}{\xi a_1}, \end{cases} \quad (48)$$

where $\tilde{\lambda}_{ij} = \frac{\Gamma_{ij}\beta_{ij}}{\tilde{\psi}_i}$.

Let, $A \triangleq min\left\{max\left\{\tilde{Y}, \tilde{Z}_1\right\}, \tilde{Z}_2\right\}$, and the corresponding CDF is obtained as,

$$F_A(a) = \begin{cases} 1 - \left(1 - \left(F_{\tilde{Y}}(a)F_{\tilde{Z}_1}(a)\right)\right) \\ \left(1 - F_{\tilde{Z}_2}(a)\right); & a < \frac{a_2}{\xi a_1}, \\ 1; & a \geq \frac{a_2}{\xi a_1}. \end{cases} \quad (49)$$

Using the random variable A, (45) can be re-written as,

$$\begin{aligned} C_{X_2} &= \frac{1}{4}\int_{f_l}^{f_u}\int_0^{\infty} \log_2(1+A) f_A(a)\, da\, df \\ &= \frac{1}{4\ln 2}\int_{f_l}^{f_u}\int_0^{\frac{a_2}{\xi a_1}} \frac{1-F_A(a)}{1+a}\, da\, df. \end{aligned} \quad (50)$$

The overall ergodic rate achieved in STBC-NOMA-CRS is given by, $\sum_{i=1}^{4} C_{X_i}$.

IV. NUMERICAL AND SIMULATION RESULTS

In this section, analytical and Monte Carlo simulation results are provided to describe our investigations on the impact of I-CSI and I-SIC on ergodic rate, outage probability and energy efficiency of the NOMA-CRS scheme. We have used Monte Carlo simulations to generate the Rayleigh fading coefficients for the channel links and MATLAB® 2018b with Phased Array System Toolbox™ to simulate the underwater channel. The results are compared with the conventional decode-and-forward based CRS scheme in UASNs [4]. From the system model, we recall that node P is far from node S with poor channel conditions and node G is close to node S with good channel conditions. Without loss of generality, we set, $D_{SG} = 0.1\, D_{SP}$, $\theta = 60°$, $a_1 = 0.95$ and $a_2 = 0.05$. The remaining parameters used for simulation and analytical

$$\tilde{V}_2 = \log_2\left(1 + min\left\{max\left\{\frac{a_2\left(\sum_{i=1}^{2}|h_{1i}|^2\,\Gamma_{1i}\right)}{a_1\xi\left(\sum_{i=1}^{2}|h_{1i}|^2\,\Gamma_{1i}\right)+\psi_2}, \left(\frac{|h_{13}|^2\,\Gamma_{13}+|h_{14}|^2\,\Gamma_{14}}{2\,\tilde{\psi}_1}\right)\right\}, \frac{a_2\left(\sum_{i=1}^{2}|h_{2i}|^2\,\Gamma_{2i}\right)}{a_1\xi\left(\sum_{i=1}^{2}|h_{2i}|^2\,\Gamma_{2i}\right)+\psi_2}\right\}\right) \quad (46)$$

TABLE 2. Parameters used for performance analysis.

System parameter	Value
Bandwidth coefficient (B)	$19.76\ dB\ re\ \mu kHz$
Bandwidth exponent (Q)	$0.59\ dB\ re\ \frac{kHz}{km}$
Transmit power consumption (P_{tx})	35 W
Receive power consumption (P_{rx})	0.7 W
Power allocation coefficient (a_1)	0.95
Threshold data rates R_1, R_2	1.5, 1.75 bpcu respectively
Spreading factor (k)	$k = 1$ for shallow water
Spreading factor (k)	$k = 2$ for deep water
Depth in km	10 m for shallow water
Depth in km	1 km for deep water
Wind speed (w)	6.67 m/s (average wind speed)
Shipping activity (s)	0.5 (average value)
Operating frequency range	1 kHz to 170 KHz
Directivity index	$0\ dB$ (omni-directional)
η_{ea}	0.7

analysis are listed in Table. 2 and these values took from Evologics® practical underwater acoustic modem [41]. First, we have analysed the impact of I-CSI considering the perfect SIC. Then, assuming perfect CSI, the impact of I-SIC on the ergodic sum rate, outage probability and energy efficiency is analysed with respect to distance between the S-P link in both shallow and deep water scenarios. Later, we have analysed the impact of the relay position on the NOMA-CRS scheme. Finally, the impact of wind speed and shipping activities on the NOMA-CRS is analysed considering realistic underwater scenario.

A. SHALLOW WATER

In this subsection, we analyse the impacts of the CSI and SIC on the ergodic sum rate, outage probability and energy efficiency with respect to the distance between the S-P link in shallow water scenario.

1) IMPACT OF CSI

Figure 3 shows the impact of CSI on the ergodic sum-rate achieved by the NOMA-CRS and CRS schemes with respect to the distance between the S-P link in shallow water scenario. In particular, it has been observed that the ergodic rate of the NOMA-CRS and CRS decreases with the increase in the distance between the S-P link. Because of the SNRs dependence on the respective transmission distance. Another important fact from Fig. 3 is that the ergodic gains achieved by the NOMA-CRS compared to CRS in UASNs are reduced by increasing the values of channel estimation error factor (*i.e.,* κ). This is because multiple symbols are transmitted in a specific time slot using superposition coding in the NOMA-CRS. As a consequence, the increase in values of channel estimation error factor has an impact on the performance of both X_1 and X_2 symbols in NOMA-CRS for UASNs.

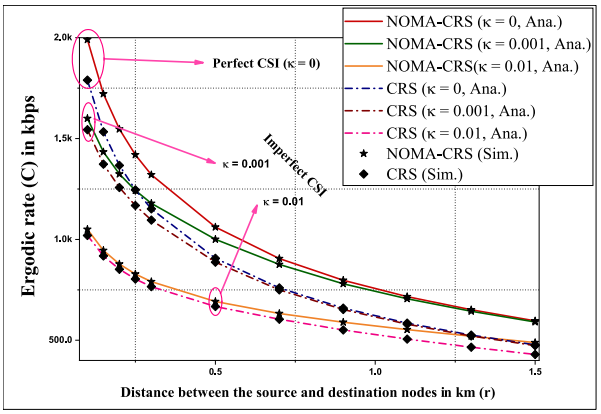

FIGURE 3. Impact of the CSI on the ergodic sum rate achieved by the NOMA-CRS and CRS schemes with respect to distance between the S-P link in shallow water: by setting $H = 10\ m$, $k = 1$, $D_{SG} = 0.1\ D_{SP}$, $\theta = 60°$, $\xi = 0$ (perfect SIC), $a_1 = 0.95$ and $a_2 = 0.05$.

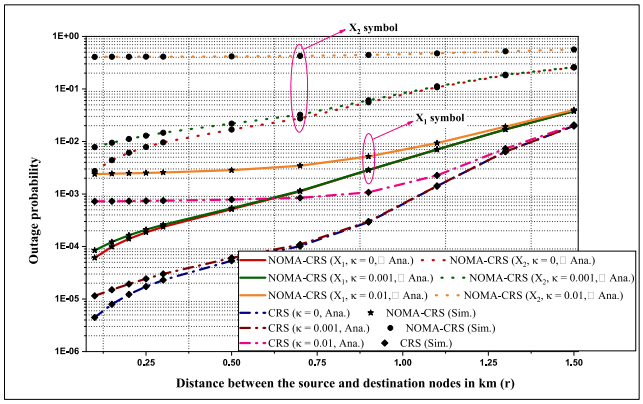

FIGURE 4. Impact of the CSI on the outage probability behaviors the NOMA-CRS and CRS schemes with respect to distance between the S-P link in shallow water: by setting $H = 10\ m$, $k = 1$, $D_{SG} = 0.1\ D_{SP}$, $\theta = 60°$, $\xi = 0$ (perfect SIC), $a_1 = 0.95$, $a_2 = 0.05$ and $R_1 = 1.5$, $R_2 = 1.75$ bits per channel usage.

Figure 4 depicts the outage probability behaviours of NOMA-CRS (*i.e.* symbols X_1 and X_2) and CRS schemes with respect to the distance between the S-P link in shallow water by setting $R_1 = 1.5$, $R_2 = 1.75$ bits per channel usage. As shown in Fig. 4, the outage behaviour of CRS is superior to that of NOMA-CRS for various distances between the S-P link. The reason behind the degradation of outage behaviour in NOMA-CRS is superposition coding, in which the X_1 symbol affects the outage behaviour of X_2 symbol and vice versa. Additionally, it can also be observed that, with the increase in values of channel estimation error factor, the outage probability behaviours of both CRS and NOMA-CRS schemes are significantly degraded. As a result, the search for efficient techniques for perfect estimation of the CSIs in UASNs is crucial, which is open to the research community.

Figure 5 plots the energy efficiency curves of NOMA-CRS and CRS schemes with respect to the distance between the S-P link in shallow water. The energy efficiency performance of NOMA-CRS is observed to be better than that of CRS for

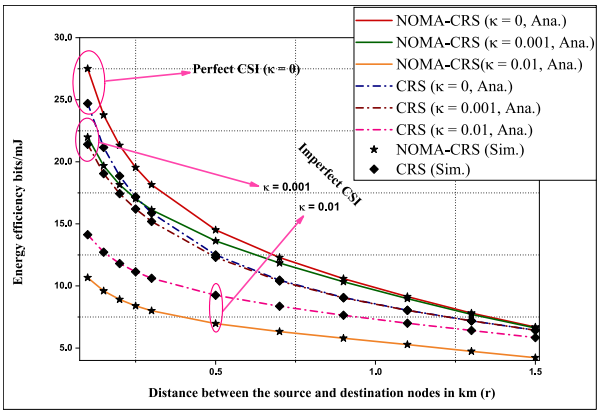

FIGURE 5. Impact of the CSI on the energy efficiency performance of the NOMA-CRS and CRS schemes with respect to the distance between the S-P link in shallow water: by setting $H = 10$ *m*, $k = 1$, $D_{SG} = 0.1\ D_{SP}$, $\theta = 60°$, $\xi = 0$ (perfect SIC), $a_1 = 0.95$, $a_2 = 0.05$ and $R_1 = 1.5$, $R_2 = 1.75$ bits per channel usage.

lower values of channel estimation error factor ($\kappa \approx 0.001$). For higher values of κ, it is observed that the energy efficiency of NOMA-CRS is degraded, and is slightly lower than that of the CRS scheme.

2) IMPACT OF SIC

Here, we analyse the performance of ergodic rate, outage probability and energy efficiency of NOMA-CRS and CRS schemes for the different levels of I-SIC (*i.e.,* by varying the SIC inefficiency factor (ξ)). It is noted from Fig. 6 that, we obtain the lowest ergodic rate performance of NOMA-CRS scheme at a high level of I-SIC (for values above $\xi = 1 \times 10^{-4}$), which is even lower than the CRS regime. It is also noted that the performance gap between the perfect SIC and the I-SIC is high at low distances between the S-P link. Figure 7 depicts the outage probability behaviour of the NOMA-CRS (*i.e.* symbols X_1 and X_2) and CRS schemes with respect to the distance between the S-P link in shallow water. It can be noted that, from the mathematical modelling presented in subsection II-B2, the impact of I-SIC only affects the outage behaviour of X_2 symbol in NOMA-CRS. It can be observed that, with the increase in the values of SIC inefficiency factor, the outage behaviour of X_2 is deteriorating, as shown in Fig. 7. Further, the outage performance of X_2 symbol is approximately the same as the perfect SIC NOMA-CRS scheme when a small amount of I-SIC occurs at $\xi = 1 \times 10^{-6}$. Figure 8 plots the energy efficiency curves of NOMA-CRS and CRS schemes with respect to the distance between the S-P link in shallow water, taking into account I-SIC. It can be seen that NOMA-CRS is able to achieve better energy efficiency compared to the CRS scheme for the case of perfect SIC and lower values of $\xi \leq 1 \times 10^{-6}$. For the case of $\xi > 1 \times 10^{-4}$, the performance of the NOMA-CRS scheme is significantly degraded and is slightly lower than the CRS scheme.

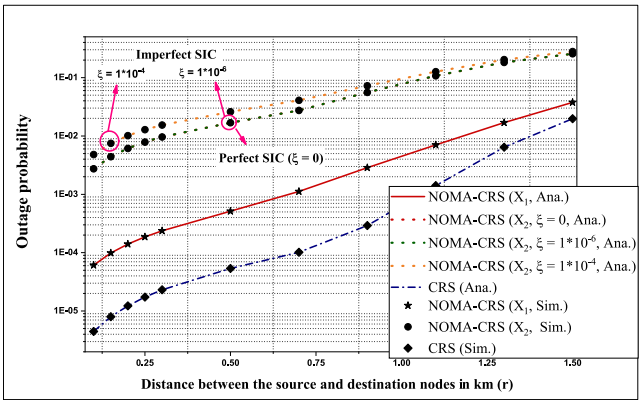

FIGURE 7. Impact of the I-SIC on the outage probability behaviours the NOMA-CRS and CRS schemes with respect to distance between the S-P link in shallow water: by setting $H = 10$ *m*, $k = 1$, $D_{SG} = 0.1\ D_{SP}$, $\theta = 60°$, $\kappa = 0$ (perfect CSI), $a_1 = 0.95$, $a_2 = 0.05$ and $R_1 = 1.5$, $= R_2 = 1.75$ bits per channel usage.

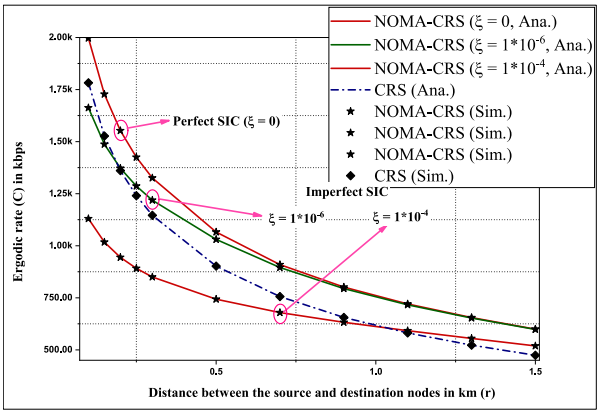

FIGURE 6. Impact of the I-SIC on the ergodic sum rate achieved by the NOMA-CRS and CRS schemes with respect to the distance between the S-P link in shallow water: by setting $H = 10$ *m*, $k = 1$, $D_{SG} = 0.1\ D_{SP}$, $\theta = 60°$, $\kappa = 0$ (perfect CSI), $a_1 = 0.95$ and $a_2 = 0.05$.

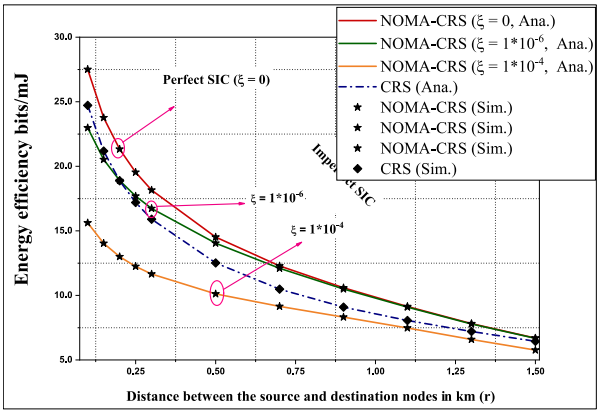

FIGURE 8. Impact of the I-SIC on the energy efficiency performance of the NOMA-CRS and CRS schemes with respect to the distance between the S-P link in shallow water: by setting $H = 10$ *m*, $k = 1$, $D_{SG} = 0.1\ D_{SP}$, $\theta = 60°$, $\kappa = 0$ (perfect CSI), $a_1 = 0.95$, $a_2 = 0.05$ and $R_1 = 1.5$, $= R_2 = 1.75$ bits per channel usage.

B. DEEP WATER

In this subsection, we analyse the impacts of the CSI and SIC on the ergodic sum rate, outage probability and energy efficiency with respect to the distance between the S-P link in deep water scenario.

1) IMPACT OF CSI

Figure 9 shows the impact of CSI on the ergodic sum rate with respect to the distance between S-P link in deep water scenario. In Fig. 9, ergodic rate response in deep water is observed to be similar to shallow water scenario. But, the ergodic rate performance has deteriorated rapidly with respect to distance when compared to shallow water scenario. This is due to the fact that, acoustic signals experience spherical spreading which results in high transmission losses in deep water. The performance of NOMA-CRS and CRS schemes have significantly deteriorated with the increase in I-CSI in deep water, as shown in Fig. 9. Figure 10 depicts the impact of CSI on the outage probability with respect to the distance between S-P link in deep water scenario. Similar to the ergodic rate performance, the outage behaviour also showed a similar response in deep water as in shallow water. However, the outage behaviour is rapidly conversing to a value one with respect to distance between S-P link in deep water. In Fig. 10, it can also be observed that the I-CSI severely affecting the performance of outage probability of NOMA-CRS and CRS schemes in deep water. Figure 11 shows the energy efficiency performance of the NOMA-CRS and CRS schemes with respect to the distance between S-P link. It can be seen that, NOMA-CRS is capable of achieving better energy efficiency compared to the CRS scheme. Further, a significant observation from Fig. 11 is that the energy efficiency shows a better performance for $d < 400\ m$, but for $d \geq 400\ m$ the energy efficiency of NOMA-CRS scheme significantly decreases due to spherical spreading.

2) IMPACT OF SIC

Figure 12 shows the effect of SIC on the ergodic sum rate with respect to the distance between the S-P link in deep water scenario. The ergodic rates of NOMA-CRS have gradually decreased with the gradual increase in the impact of SIC in deep water similar to the shallow water scenario. Figure 13 depicts the impact of SIC on the outage probability with respect to the distance between the S-P link in deep water scenario. The increase in the SIC imperfections has a substantial decrease in the outage probability of X_2 symbol of NOMA-CRS. Figure 14 shows the impact of SIC on energy efficiency with respect to the distance between the S-P link in deep water scenario. It can be seen that NOMA-CRS is capable of achieving better energy efficiency compared to the CRS scheme for the lower values of the SIC inefficiency factor up to $\xi = 1 \times 10^{-6}$. Further, it can be observed from Fig. 14 that the energy efficiency performance is better for $d < 400\ m$, but for $d \geq 400\ m$ the energy efficiency of NOMA-CRS scheme significantly decreases due to spherical spreading. Finally, it can be observed that the SIC also has an impact similar to shallow water scenario on the ergodic rate,

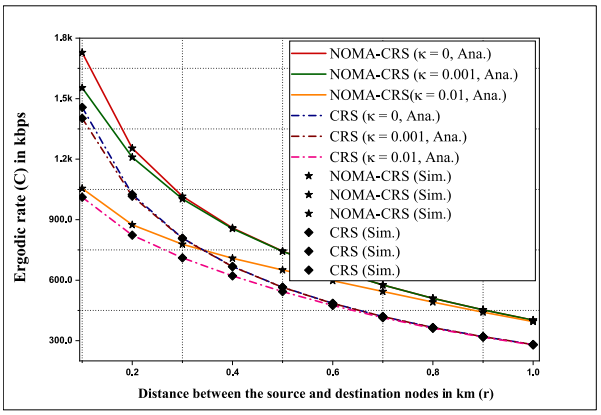

FIGURE 9. Impact of the I-CSI on the ergodic sum rate achieved by the NOMA-CRS and CRS schemes with respect to distance between the S-P link in deep water: by setting $H = 1000\ m$, $k = 2$, $D_{SG} = 0.1\ D_{SP}$, $\theta = 60°$, $\xi = 0$ (perfect SIC), $a_1 = 0.95$ and $a_2 = 0.05$.

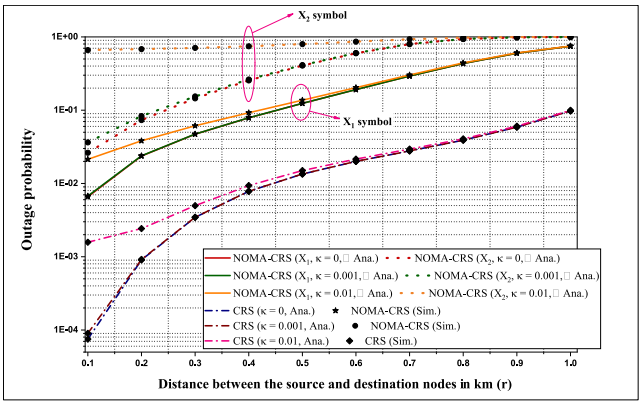

FIGURE 10. Impact of the I-CSI on the outage probability behaviours the NOMA-CRS and CRS schemes with respect to distance between the S-P link in deep water: by setting $H = 1000\ m$, $k = 2$, $D_{SG} = 0.1\ D_{SP}$, $\theta = 60°$, $\xi = 0$ (perfect SIC), $a_1 = 0.95$, $a_2 = 0.05$ and $R_1 = 1.5$, $R_2 = 1.75$ bits per channel usage.

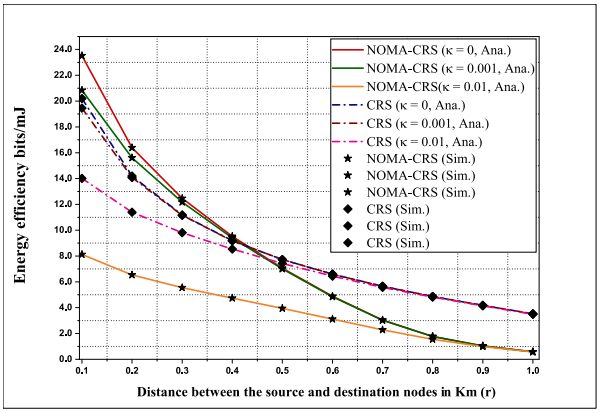

FIGURE 11. Impact of the I-CSI on the energy efficiency performance of the NOMA-CRS and CRS schemes with respect to the distance between the S-P link in deep water: by setting $H = 1000\ m$, $k = 2$, $D_{SG} = 0.1\ D_{SP}$, $\theta = 60°$, $\xi = 0$ (perfect SIC), $a_1 = 0.95$, $a_2 = 0.05$ and $R_1 = 1.5$, $R_2 = 1.75$ bits per channel usage.

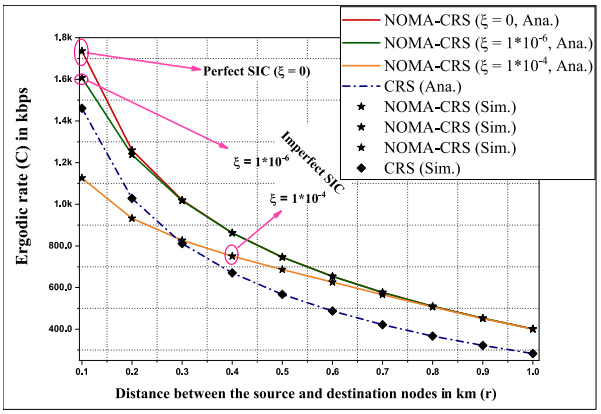

FIGURE 12. Impact of the I-SIC on the ergodic sum rate achieved by the NOMA-CRS and CRS schemes with respect to the distance between the S-P link in deep water: by setting $H = 1000$ m, $k = 2$, $D_{SG} = 0.1$ D_{SP}, $\theta = 60°$, $\kappa = 0$ (perfect CSI), $a_1 = 0.95$ and $a_2 = 0.05$.

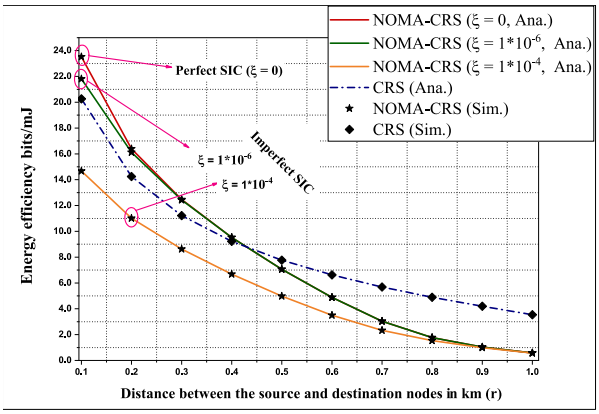

FIGURE 14. Impact of the I-SIC on the energy efficiency performance of the NOMA-CRS and CRS schemes with respect to the distance between the S-P link in deep water: by setting $H = 1000$ m, $k = 2$, $D_{SG} = 0.1$ D_{SP}, $\theta = 60°$, $\kappa = 0$ (perfect CSI), $a_1 = 0.95$, $a_2 = 0.05$ and $R_1 = 1.5$, $R_2 = 1.75$ bits per channel usage.

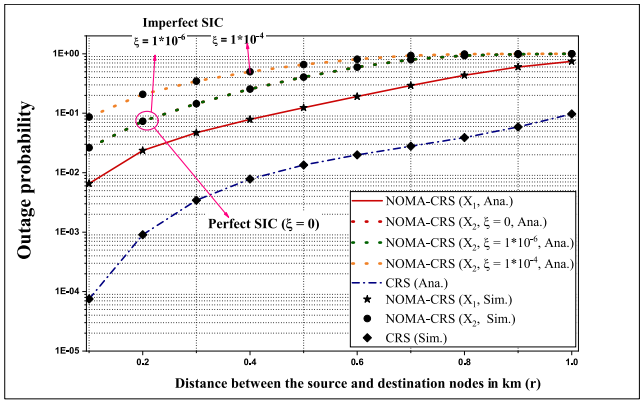

FIGURE 13. Impact of the I-SIC on the outage probability behaviours the NOMA-CRS and CRS schemes with respect to distance between the S-P link in deep water: by setting $H = 1000$ m, $k = 2$, $D_{SG} = 0.1$ D_{SP}, $\theta = 60°$, $\kappa = 0$ (perfect CSI), $a_1 = 0.95$, $a_2 = 0.05$ and $R_1 = 1.5$, $R_2 = 1.75$ bits per channel usage.

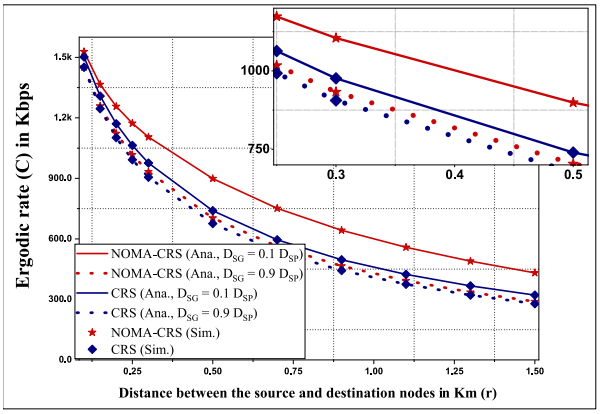

FIGURE 15. Impact of the position of the relay node on the ergodic sum rate achieved by the NOMA-CRS and CRS schemes with respect to the distance between the S-P link in underwater: by setting $k = 1.5$, $\theta = 60°$, $(\xi, \kappa) = (1 \times 10^{-6}, 1 \times 10^{-3})$, $a_1 = 0.95$, and $a_2 = 0.05$.

outage probability, and energy efficiency of NOMA-CRS in deep water.

It can be concluded from both the shallow and deep water scenarios that, the performance of NOMA-CRS is significantly affected by the CSI estimation error factor compared to the CSR scheme. As a result, there exists a trade-off between the ergodic rate and the energy efficiency because of outage probability dependence on CSI estimation error factor. As the technological advances in the CSI estimation techniques rapidly evolving will guarantee the performance enhancement of the NOMA-CRS scheme. Further, there is a need for efficient SIC techniques are required to get higher performance gains of NOMA-CRS scheme compared to the CRS scheme.

3) IMPACT OF RELAY POSITION

In this subsection, the ergodic rate performance of NOMA-CRS and CRS schemes are analysed with the change in the position of the relay node in a practical underwater scenario. Here, the relay node position is changed using $D_{SG} = 0.1\ D_{SP}$ (node G is existed near to the node S compared to P), and $D_{SG} = 0.9\ D_{SP}$ (node G is existed near to the node P compared to S) by setting $\theta = 60°$. It is noted from Fig. 15 that, the ergodic rate performance of NOMA-CRS approaching to ergodic rate performance of CRS, when the relay node is moves away from the source node. It is also evident that NOMA-CRS is capable of achieving higher ergodic rates even in the practical scenario in which impacts of both I-CSI and I-SIC are considered.

4) IMPACT OF ENVIRONMENTAL EFFECTS NAMELY, WIND SPEED AND SHIPPING ACTIVITY

In this subsection, we discussed the performance analysis of NOMA-CRS in terms of ergodic sum rate by considering the effects of environmental parameters, namely shipping noises, and wind speed (surface motion). The wind speed (w) mainly varies approximately in the range of $1 - 60$ m/s. The shipping noise depends on shipping activity factor (s), which varies in the range of [0, 1], where 0 and 1 represent

TABLE 3. Ergodic rate (in kbps) analysis of STBC-NOMA-CRS and NOMA-CRS.

Transmission Distance		0.1 km		1 km		1.5 km	
Scheme		STBC-NOMA-CRS	NOMA-CRS	STBC-NOMA-CRS	NOMA-CRS	STBC-NOMA-CRS	NOMA-CRS
$\kappa = 0, \xi = 0$	Shallow water	2030.5	1983.2	796.4	752.8	635.3	595.3
$\kappa = 1 \times 10^{-3}, \xi = 1 \times 10^{-6}$	Shallow water	1551.7	1533.4	780.1	736.9	629.3	589.8
Transmission Distance		0.1 km		0.5 km		1 km	
$\kappa = 0, \xi = 0$	Deep water	1820.5	1734.2	786.0	746.6	448.4	447.9
$\kappa = 1 \times 10^{-3}, \xi = 1 \times 10^{-6}$	Deep water	1555.4	1502.6	785.5	745.6	447.5	401.9

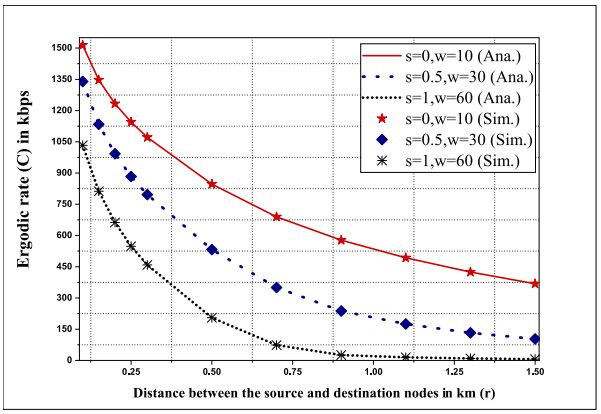

FIGURE 16. Impact of environmental effects namely, wind speed and shipping activity on the ergodic sum rate achieved by the NOMA-CRS and CRS schemes with respect to distance between the S-P link: by setting $k = 1.5$, $D_{SG} = 0.1\ D_{SP}$, $\theta = 60°$, $(\xi, \kappa) = (1 \times 10^{-6}, 1 \times 10^{-3})$, $a_1 = 0.95$, and $a_2 = 0.05$.

low and high shipping activities, respectively [36]. As a result, we formed three different pairs of wind velocities and shipping activities as shown in Fig. 16. It is evident from the results that high-speed winds and high shipping activities severely degrade the performance of ergodic sum rate of the NOMA-CRS.

5) COMPARATIVE ANALYSIS OF STBC-NOMA-CRS AND NOMA-CRS

In this subsection, we compare the performance of STBC-NOMA-CRS and NOMA-CRS schemes, as shown in Table 3. In NOMA-CRS, we assume that perfect CSI is available at the transmitter. From the results, it is evident that the STBC-NOMA-CRS is able to provide the same performance of NOMA-CRS scheme, even without the CSI at the transmitter. A slight improvement in the ergodic rate performance is also observed as shown in Table 3. It is due to the benefits of both spectral efficiency and transmit diversity, which makes this scheme perfectly suitable for practical UASNs.

V. CONCLUSION

The objective of this research work is to improve the performance of cooperative relaying strategy in UASNs by incorporating NOMA. We have proposed a NOMA-CRS scheme for enhancing the performance of the bandwidth-limited and energy-constrained UASNs. Mathematical expressions for ergodic rate, outage probability and energy efficiency for NOMA-CRS were derived by considering underwater specific channel characteristics. Impact of imperfect channel state information (I-CSI) and imperfect successive interference cancellation (I-SIC) on the performance of NOMA-CRS is thoroughly investigated. From the analytical and simulation results, it can be observed that NOMA-CRS can achieve significant improvement in ergodic sum rate and energy efficiency, at the cost of a slight degradation in the outage performance. I-CSI and I-SIC have considerable influence on the performance of NOMA-CRS. The performance of NOMA-CRS in UASNs is better when the relay node is placed near to the source node. Finally, we have analysed the impact of environmental effects, namely wind speed and shipping activities on the NOMA-CRS. From the results, it is observed that that high-speed winds and high shipping activities can severely degrade the performance of ergodic sum rate and energy efficiency of the NOMA-CRS. Finally, we have proposed STBC-NOMA-CRS for UASNs. From the results, it is evident that this scheme can provide performance enhancement same as NOMA-CRS ascheme for UASNs, without transmitter CSI.

REFERENCES

[1] M. Jouhari, K. Ibrahimi, H. Tembine, and J. Ben-Othman, "Underwater wireless sensor networks: A survey on enabling technologies, localization protocols, and Internet of underwater things," *IEEE Access*, vol. 7, pp. 96879–96899, 2019.

[2] C.-C. Kao, Y.-S. Lin, G.-D. Wu, and C.-J. Huang, "A comprehensive study on the Internet of underwater things: Applications, challenges, and channel models," *Sensors*, vol. 17, no. 7, p. 1477, Jun. 2017. [Online]. Available: https://www.mdpi.com/1424-8220/17/7/1477

[3] M. C. Domingo, "An overview of the Internet of underwater things," *J. Netw. Comput. Appl.*, vol. 35, no. 6, pp. 1879–1890, 2012. [Online]. Available: http://www.sciencedirect.com/science/article/pii/S1084804512001646

[4] S. Al-Dharrab, M. Uysal, and T. M. Duman, "Cooperative underwater acoustic communications [accepted from open call]," *IEEE Commun. Mag.*, vol. 51, no. 7, pp. 146–153, Jul. 2013.

[5] L. Dai, B. Wang, Y. Yuan, S. Han, I. Chih-Lin, and Z. Wang, "Non-orthogonal multiple access for 5G: Solutions, challenges, opportunities, and future research trends," *IEEE Commun. Mag.*, vol. 53, no. 9, pp. 74–81, Sep. 2015.

[6] Y. Liu, Z. Qin, M. Elkashlan, Z. Ding, A. Nallanathan, and L. Hanzo, "Nonorthogonal multiple access for 5G and beyond," *Proc. IEEE*, vol. 105, no. 12, pp. 2347–2381, Dec. 2017.

[7] E. G. Larsson, O. Edfors, F. Tufvesson, and T. L. Marzetta, "Massive MIMO for next generation wireless systems," *IEEE Commun. Mag.*, vol. 52, no. 2, pp. 186–195, Feb. 2014.

[8] L. Lu, G. Y. Li, A. L. Swindlehurst, A. Ashikhmin, and R. Zhang, "An overview of massive MIMO: Benefits and challenges," *IEEE J. Sel. Topics Signal Process.*, vol. 8, no. 5, pp. 742–758, Oct. 2014.

[9] S. M. R. Islam, N. Avazov, O. A. Dobre, and K.-S. Kwak, "Power-domain non-orthogonal multiple access (NOMA) in 5G systems: Potentials and challenges," *IEEE Commun. Surveys Tuts.*, vol. 19, no. 2, pp. 721–742, 2nd Quart., 2017.
[10] L. Ma, S. Zhou, G. Qiao, S. Liu, and F. Zhou, "Superposition coding for downlink underwater acoustic OFDM," *IEEE J. Ocean. Eng.*, vol. 42, no. 1, pp. 175–187, Jan. 2017.
[11] Ahmad and Chang, "Downlink power allocation strategy for next-generation underwater acoustic communications networks," *Electronics*, vol. 8, no. 11, p. 1297, Nov. 2019.
[12] M. Jain, N. Sharma, A. Gupta, D. Rawal, and P. Garg, "Performance analysis of NOMA assisted underwater visible light communication system," *IEEE Wireless Commun. Lett.*, vol. 9, no. 8, pp. 1291–1294, Aug. 2020.
[13] M. J. Bocus, D. Agrafiotis, and A. Doufexi, "Non-orthogonal multiple access (NOMA) for underwater acoustic communication," in *Proc. IEEE 88th Veh. Technol. Conf. (VTC-Fall)*, Aug. 2018, pp. 1–5.
[14] E. A. Makled, A. Yadav, O. A. Dobre, and R. D. Haynes, "Hierarchical full-duplex underwater acoustic network: A NOMA approach," in *Proc. OCEANS MTS/IEEE Charleston*, Oct. 2018, pp. 1–6.
[15] J.-B. Kim and I.-H. Lee, "Capacity analysis of cooperative relaying systems using non-orthogonal multiple access," *IEEE Commun. Lett.*, vol. 19, no. 11, pp. 1949–1952, Nov. 2015.
[16] Z. Ding, M. Peng, and H. V. Poor, "Cooperative non-orthogonal multiple access in 5G systems," *IEEE Commun. Lett.*, vol. 19, no. 8, pp. 1462–1465, Aug. 2015.
[17] Y. Zhang, Z. Yang, Y. Feng, and S. Yan, "Performance analysis of cooperative relaying systems with power-domain non-orthogonal multiple access," *IEEE Access*, vol. 6, pp. 39839–39848, Jul. 2018.
[18] Y. Chen, X. Jin, L. Wan, X. Zhang, and X. Xu, "Selective dynamic coded cooperative communications for multi-hop underwater acoustic sensor networks," *IEEE Access*, vol. 7, pp. 70552–70563, 2019.
[19] Z. Liu, F. Bai, and L. Song, "Underwater decode-interleave-forward cooperative strategy for underwater acoustic communication," *IEEE Access*, vol. 7, pp. 19698–19708, 2019.
[20] A. Ghosh, J.-W. Lee, and H.-S. Cho, "Throughput and energy efficiency of a cooperative hybrid ARQ protocol for underwater acoustic sensor networks," *Sensors*, vol. 13, no. 11, pp. 15385–15408, Nov. 2013. [Online]. Available: https://www.mdpi.com/1424-8220/13/11/15385
[21] V. Goutham and V. P. Harigovindan, "Modeling and analysis of hybrid ARQ scheme for incremental cooperative communication in underwater acoustic sensor networks," *Iranian J. Sci. Technol., Trans. Electr. Eng.*, vol. 45, no. 1, pp. 279–294, Mar. 2021.
[22] R. Wang, A. Yadav, E. A. Makled, O. A. Dobre, R. Zhao, and P. K. Varshney, "Optimal power allocation for full-duplex underwater relay networks with energy harvesting: A reinforcement learning approach," *IEEE Wireless Commun. Lett.*, vol. 9, no. 2, pp. 223–227, Feb. 2020.
[23] D. D. Tan and D.-S. Kim, "Cooperative transmission scheme for multi-hop underwater acoustic sensor networks," *Int. J. Commun. Netw. Distrib. Syst.*, vol. 14, no. 1, pp. 1–18, Nov. 2015, doi: 10.1504/IJCNDS.2015.065998.
[24] R. Cao, F. Qu, and L. Yang, "Asynchronous amplify-and-forward relay communications for underwater acoustic networks," *IET Commun.*, vol. 10, no. 6, pp. 677–684, Apr. 2016.
[25] S. Al-Dharrab, A. Muqaibel, and M. Uysal, "Performance of multicarrier cooperative communication systems over underwater acoustic channels," *IET Commun.*, vol. 11, no. 12, pp. 1941–1951, Aug. 2017.
[26] M. A. Rahman, Y. Lee, and I. Koo, "EECOR: An energy-efficient cooperative opportunistic routing protocol for underwater acoustic sensor networks," *IEEE Access*, vol. 5, pp. 14119–14132, 2017.
[27] A. Yahya, S. U. Islam, M. Zahid, G. Ahmed, M. Raza, H. Pervaiz, and F. Yang, "Cooperative routing for energy efficient underwater wireless sensor networks," *IEEE Access*, vol. 7, pp. 141888–141899, 2019.
[28] S. Ghoreyshi, A. Shahrabi, and T. Boutaleb, "A novel cooperative opportunistic routing scheme for underwater sensor networks," *Sensors*, vol. 16, no. 3, p. 297, Feb. 2016. [Online]. Available: https://www.mdpi.com/1424-8220/16/3/297
[29] H. Tran-Dang and D.-S. Kim, "Channel-aware energy-efficient two-hop cooperative routing protocol for underwater acoustic sensor networks," *IEEE Access*, vol. 7, pp. 63181–63194, 2019.
[30] M. C. Domingo and R. Prior, "Energy analysis of routing protocols for underwater wireless sensor networks," *Comput. Commun.*, vol. 31, no. 6, pp. 1227–1238, Apr. 2008. [Online]. Available: http://www.sciencedirect.com/science/article/pii/S0140366407004689
[31] R. J. Urick, *Principles Of Underwater Sound*, 3rd ed. Los Altos, CA, USA: Peninsula Publishing, 1983.
[32] K. V. Mackenzie, "Nine-term equation for sound speed in the oceans," *J. Acoust. Soc. Amer.*, vol. 70, no. 3, pp. 807–812, Sep. 1981.
[33] K. S. Geethu and A. V. Babu, "A hybrid ARQ scheme combining erasure codes and selective retransmissions for reliable data transfer in underwater acoustic sensor networks," *EURASIP J. Wireless Commun. Netw.*, vol. 2017, no. 1, p. 32, Dec. 2017.
[34] R. E. Francois and G. R. Garrison, "Sound absorption based on ocean measurements: Part I: Pure water and magnesium sulfate contributions," *J. Acoust. Soc. Amer.*, vol. 72, no. 3, pp. 896–907, Sep. 1982, doi: 10.1121/1.388170.
[35] R. E. Francois and G. R. Garrison, "Sound absorption based on ocean measurements. Part II: Boric acid contribution and equation for total absorption," *J. Acoust. Soc. Amer.*, vol. 72, no. 6, pp. 1879–1890, Dec. 1982, doi: 10.1121/1.388673.
[36] M. Stojanovic, "On the relationship between capacity and distance in an underwater acoustic communication channel," in *Proc. 1st ACM Int. workshop Underwater Netw. (WUWNet)*, New York, NY, USA, 2006, pp. 41–47.
[37] Y. Zhang, R. Venkatesan, O. A. Dobre, and C. Li, "Efficient estimation and prediction for sparse time-varying underwater acoustic channels," *IEEE J. Ocean. Eng.*, vol. 45, no. 3, pp. 1112–1125, Jul. 2019.
[38] Y. Zhou and F. Tong, "Channel estimation based equalizer for underwater acoustic Multiple-Input-Multiple-Output communication," *IEEE Access*, vol. 7, pp. 79005–79016, 2019.
[39] D. Zwillinger, V. Moll, I. Gradshteyn, and I. Ryzhik, Eds., "3-4—Definite integrals of elementary functions," in *Table of Integrals, Series, and Products*, 8th ed. Boston, MA, USA: Academic, 2015, pp. 249–519.
[40] X. Yue, Y. Liu, S. Kang, A. Nallanathan, and Y. Chen, "Modeling and analysis of two-way relay non-orthogonal multiple access systems," *IEEE Trans. Commun.*, vol. 66, no. 9, pp. 3784–3796, Sep. 2018.
[41] *Underwater Acoustic Modems*. Accessed: Nov. 17, 2020. [Online]. Available: https://evologics.de/acoustic-modems

VEERAPU GOUTHAM (Member, IEEE) received the bachelor's degree in electronics and communication engineering from Sri Krishnadevaraya University, Anantapur, and the master's degree in digital communications from the National Institute of Technology Bhopal, India. He is currently pursuing the Ph.D. degree with the Department of Electronics and Communication Engineering, National Institute of Technology Puducherry, India. His research interests include wireless networks, wireless communications, and underwater acoustic sensor networks.

V. P. HARIGOVINDAN (Senior Member, IEEE) received the B.Tech. degree in electronics and communication engineering from the University of Calicut, the M.Tech. degree (with First Rank) in digital electronics and communication systems from Visvesvaraya Technological University, and the Ph.D. degree from the National Institute of Technology Calicut, in 2013. He is currently an Assistant Professor with the Department of Electronics and Communication Engineering and an Associate Dean (Faculty Welfare) with the National Institute of Technology Puducherry (under Ministry of Education, Government of India). He has more than 25 International publications to his credit. He is currently serving as the Principal Investigator for two funded projects one from the Department of Science and Technology, Government of India, and one from the Science and Engineering Research Board. His research interests include wireless networks and wireless communications.